Development/Plasticity/Repair

# STIM1 Is Required for Remodeling of the Endoplasmic Reticulum and Microtubule Cytoskeleton in Steering Growth Cones

Macarena Pavez,[1*] Adrian C. Thompson,[1*] Hayden J. Arnott,[1] Camilla B. Mitchell,[2] Ilaria D'Atri,[3] Emily K. Don,[4] John K. Chilton,[3] Ethan K. Scott,[5,6] John Y. Lin,[1] Kaylene M. Young,[2] Robert J. Gasperini,[1†] and Lisa Foa[1†]

[1]School of Medicine, [2]Menzies Institute of Medical Research, University of Tasmania, Hobart, 7001 Tasmania, Australia, [3]University of Exeter Medical School, Wellcome Wolfson Centre for Medical Research, University of Exeter, Exeter EX2 5DW, United Kingdom, [4]Centre for Motor Neuron Disease Research, Department of Biomedical Sciences, Macquarie University, Macquarie Park, 2109 New South Wales, Australia, [5]School of Biomedical Sciences, and [6]Queensland Brain Institute, University of Queensland, St. Lucia, 4072 Queensland, Australia

The spatial and temporal regulation of calcium signaling in neuronal growth cones is essential for axon guidance. In growth cones, the endoplasmic reticulum (ER) is a significant source of calcium signals. However, it is not clear whether the ER is remodeled during motile events to localize calcium signals in steering growth cones. The expression of the ER-calcium sensor, stromal interacting molecule 1 (STIM1) is necessary for growth cone steering toward the calcium-dependent guidance cue BDNF, with STIM1 functioning to sustain calcium signals through store-operated calcium entry. However, STIM1 is also required for growth cone steering away from semaphorin-3a, a guidance cue that does not activate ER-calcium release, suggesting multiple functions of STIM1 within growth cones (Mitchell et al., 2012). STIM1 also interacts with microtubule plus-end binding proteins EB1/EB3 (Grigoriev et al., 2008). Here, we show that STIM1 associates with EB1/EB3 in growth cones and that STIM1 expression is critical for microtubule recruitment and subsequent ER remodeling to the motile side of steering growth cones. Furthermore, we extend our data *in vivo*, demonstrating that zSTIM1 is required for axon guidance in actively navigating zebrafish motor neurons, regulating calcium signaling and filopodial formation. These data demonstrate that, in response to multiple guidance cues, STIM1 couples microtubule organization and ER-derived calcium signals, thereby providing a mechanism where STIM1-mediated ER remodeling, particularly in filopodia, regulates spatiotemporal calcium signals during axon guidance.

*Key words:* axon guidance; calcium; endoplasmic reticulum; microtubule; optogenetic; STIM1

**Significance Statement**

Defects in both axon guidance and endoplasmic reticulum (ER) function are implicated in a range of developmental disorders. During neuronal circuit development, the spatial localization of calcium signals controls the growth cone cytoskeleton to direct motility. We demonstrate a novel role for stromal interacting molecule 1 (STIM1) in regulating microtubule and subsequent ER remodeling in navigating growth cones. We show that STIM1, an activator of store-operated calcium entry, regulates the dynamics of microtubule-binding proteins EB1/EB3, coupling ER to microtubules, within filopodia, thereby steering growth cones. The STIM1-microtubule-ER interaction provides a new model for spatial localization of calcium signals in navigating growth cones in the nascent nervous system.

## Introduction

A key determinant of axon guidance is the precise regulation of growth cone motility by the second messenger molecule calcium (Cohan et al., 1987; Gomez and Spitzer, 1999; Zheng, 2000; Wen et al., 2004). How the spatial localization of calcium signals is regulated to control the cytoskeleton, and therefore growth cone

Received Sept. 27, 2018; revised April 3, 2019; accepted April 4, 2019.

Author contributions: M.P., A.C.T., H.J.A., C.B.M., E.K.D., and R.J.G. performed research; M.P., A.C.T., H.J.A., C.B.M., J.Y.L., K.M.Y., R.J.G., and L.F. analyzed data; M.P., A.C.T., and R.J.G. wrote the first draft of the paper; M.P., A.C.T., J.K.C., E.K.S., J.Y.L., K.M.Y., R.J.G., H.J.A., and L.F. edited the paper; I.D., J.K.C., and E.K.S. contributed unpublished reagents/analytic tools; R.J.G. and L.F. designed research; R.J.G. and L.F. wrote the paper.

This work was supported by the Australian Government Postgraduate Awards to M.P., A.C.T., H.J.A., and C.B.M.; National Health and Medical Research Council Australia Grant 1024145 to L.F. and R.J.G., Grant 1066025 to K.M.Y.,

motility, is not well understood. Calcium-dependent guidance cues activate the release of calcium from the endoplasmic reticulum (ER) through inositol triphosphate or ryanodine receptor activation, and this mobilization of ER-calcium is key to the transduction of filopodial calcium transients necessary for axon guidance (Gu and Spitzer, 1995; Davenport et al., 1996; Gomez and Spitzer, 2000; Ooashi et al., 2005; Tojima et al., 2011; Mitchell et al., 2012). The morphology and subcellular distribution of ER are highly regulated and yet dynamic (Zhang and Hu, 2016; Wu et al., 2017). While ER remodeling in motile growth cones has not been previously described, it is probable that the spatial translocation of ER and its ability to sustain spatially restricted calcium signals are important in regulating growth cone motility (Davenport et al., 1996; Ooashi et al., 2005; Zhang and Forscher, 2009; Mitchell et al., 2012). Understanding the molecular mechanisms that regulate the spatial localization of ER-mediated calcium signals is vital, given that defects in calcium signaling and ER function are implicated in a range of neural developmental disorders, spastic paraplegias, and neurodegeneration (Blackstone, 2012; Beetz et al., 2013; Schmunk et al., 2015, 2017).

Stromal interacting molecule 1 (STIM1) is a calcium-sensing protein located on the ER membrane. STIM1 regulates ER-calcium concentration by interacting with Orai proteins at the plasma membrane, to trigger calcium influx via store-operated calcium entry (SOCE) (Roos et al., 2005; Feske et al., 2006; Luik et al., 2006). STIM1 is required for growth cone steering in response to BDNF, netrin-1, and semaphorin-3a (sema-3a) (Mitchell et al., 2012; Shim et al., 2013). The requirement for STIM1 function in BDNF and netrin-1-induced growth cone turning was predicted, given that turning toward both guidance cues requires ER-calcium release (Li et al., 1999; Ming et al., 1999; Hong et al., 2000). However, sema-3a-induced growth cone repulsion does not require ER-mediated calcium signaling (Ming et al., 1999; Togashi et al., 2008), raising the possibility that STIM1 regulates more than SOCE and ER-calcium homeostasis in growth cones. Significantly, in cell lines, STIM1 has also been shown to interact with the microtubule cytoskeleton through end-binding proteins 1 and 3 (EB1 and EB3) (Grigoriev et al., 2008; Honnappa et al., 2009; Asanov et al., 2013). The STIM1-EB interaction sequesters STIM1 to microtubules to prevent excessive activation of SOCE (Chang et al., 2018) and is also thought to be important in localizing calcium signals in migrating endothelial cells (Tsai et al., 2014). Hence, we hypothesized that, in a highly dynamic structure, such as the neuronal growth cone, a STIM1-EB interaction could represent an important, novel mechanism for regulating the localization and remodeling of ER membranes and sustaining localized calcium signals.

We sought to determine whether the STIM1-EB interaction regulates the spatial and temporal distribution of the ER and cytoskeleton in steering growth cones. We report that STIM1 localizes with EB1/EB3 in filopodia and is required for microtubule recruitment to the motile side of turning growth cones, including the protrusion of microtubule plus tips and associated ER into filopodia. We also find that this requirement for STIM1 persists *in vivo* and is necessary for the guidance of pioneer spinal motor neurons in developing zebrafish. Perturbing STIM1 function *in vivo* resulted in growth cones extending fewer filopodia and exhibiting aberrant calcium transient activity at key navigational choice points. Our data demonstrate that STIM1 plays a crucial role in regulating the spatial distribution of ER-calcium signals and the cytoskeleton, thus controlling growth cone motility during axon guidance.

## Materials and Methods

*Animals.* All animal procedures were conducted under the approval of the University of Tasmania Animal Ethics Committee and the Macquarie University Animal Ethics Committee, in accordance with the Australian National Health and Medical Research Council Code of Practice for the Care and Use of Animals for Scientific Purposes. Embryonic Sprague Dawley rats (University of Tasmania, Hobart, Tasmania, Australia; and Macquarie University, Macquarie Park, New South Wales, Australia) and embryonic zebrafish (University of Tasmania, Australia) were used. Zebrafish lines were Gal4$^{s1020t}$/UAS:mCherry (Scott and Baier, 2009; Heap et al., 2013) and Gal4$^{s1020t}$/UAS:GCaMP5G (Scott and Baier, 2009; Thompson et al., 2016).

*Primary DRG sensory neuron culture.* Primary cultures from DRG sensory neurons were prepared as previously described (Gasperini et al., 2009; Mitchell et al., 2012). Briefly, thoracic DRG from E16-E18 Sprague Dawley rat embryos were mechanically dissociated and plated at low density onto poly-L-ornithine (1 mg/ml) and laminin (50 $\mu$g/ml)-coated glass coverslips in sensory neuron media (SNM): DMEM F-12 medium 1:1, penicillin-streptomycin (100 $\mu$g/ml), N2 neural medium supplement (1%v/v), FCS (5% v/v), and nerve growth factor (50 ng/ml). Cultures were maintained at 37°C in 5% $CO_2$ humidified incubator for 4–6 h before imaging.

In vitro *growth cone turning assay.* Growth cone turning assays were performed as previously described (Gasperini et al., 2009; Mitchell et al., 2012). Guidance cues used were BDNF human (catalog #B3795, Sigma-Aldrich) and sema-3a (catalog #1250-S3, R&D Systems).

*Transfection and protein knockdown* in vitro. Rat Neuron Nucleofection (catalog #VPG-1003, Lonza Walkersville) was used to transfect DRG neurons. Neurons were transfected with plasmids and morpholinos simultaneously. Morpholinos (Gene Tools) were STIM1-specific (5′-GGGCAAGACGAGCGCACACATCCAT) or 5′ mispaired control morpholinos (5′-GGcCAAcACcAGCcACAgATCCAT). Plasmids included the following: OptoSTIM1 (Addgene, plasmid #70160) (Kyung et al., 2015), LOVS1K (Addgene, plasmid #31981) (Pham et al., 2011), OptoSTIM1Cry2(D387A) (Addgene, plasmid #70159) (Kyung et al., 2015), pclink-BiP-mCherry-KDEL (based on Zurek et al., 2011), EB3-tdTomato (Addgene, plasmid #50708) (Merriam et al., 2013), and ER-GCaMP6-150 (gift of Prof. Tim Ryan) (de Juan-Sanz et al., 2017). EB3-YFP was transfected using nucleofection (Lonza Walkersville) or with magnetic particles following the manufacturer's instructions (NeuroMag; catalog #NM50200, Oz Biosciences) or subcloned into BamHI and NheI restriction sites of a second-generation lentiviral construct containing the neuron-specific hSyn promoter. In Figure 5, where morpholinos and siRNA were not cotransfected with a plasmid, they were introduced in the dissociation step of culturing method (see primary DRG sensory neuron culture). Cells were mechanically dissociated (before plating) in the presence of morpholino at 5 $\mu$M in SNM, or Orai1 siRNA 10 nM in SNM (catalog #304496, Alias: RGD1311873, Millenium Science), as previously described (Mitchell et al., 2012). Knockdown of protein expression was confirmed by immunocytochemistry.

*Immunocytochemistry.* Immunocytochemistry was performed as previously described (Mitchell et al., 2012). Briefly, DRG neuronal cultures were fixed in ice-cold methanol (100%) at −20°C for 15 min and 4% PFA in PBS at room temperature for 5 min, and then immunostained for STIM1 (1:500 rabbit anti-STIM1, catalog #S6072; RRID:AB_1079008, Sigma-Aldrich), $\beta$3-tubulin (1:1000 mouse anti-$\beta$3-tubulin, catalog

R.J.G., and L.F., and Grant 1165616 to L.F., J.Y.L. and R.J.G.; the University of Tasmania to R.J.G.; the Ian Potter Foundation to L.F.; and the Snow Foundation to E.K.D. We thank Prof. Tim Ryan for generously gifting plasmids; Prof. David Small for the early review of the work; and colleagues from the L.F., K.M.Y., J.Y.L., and Prof. David Small laboratories for valuable comments and suggestions.

The authors declare no competing financial interests.

*M.P. and A.C.T. contributed equally to this work.

†R.J.G. and L.F. contributed equally to this work as senior authors.

Correspondence should be addressed to Lisa Foa at lisa.foa@utas.edu.au.

A.C. Thompson's present address: Department of Neuroscience, Brown University, Providence, RI 02912.

C.B. Mitchell's present address: Division of Cancer Research, Peter MacCallum Cancer Centre, Melbourne, 3000 Victoria, Australia.

https://doi.org/10.1523/JNEUROSCI.2496-18.2019

Copyright © 2019 the authors

#G7121; RRID:AB_430874, Promega), EB3 (1:500 rat anti-EB3 [KT36], catalog #ab53360; RRID:AB_880026, Abcam), or drebrin (1:500 mouse anti-Drebrin (MF26), catalog #ADI-NBA-110-E; RRID:AB_2039073, Enzo Life Sciences) in blocking solution (5% FCS in PBS) overnight at 4°C. Following three 10 min PBS washes, primary antibodies were detected using AlexaFluor-405/-488/-568/-647 secondary antibodies (1:1000, Invitrogen) incubated for 1 h at room temperature. To assess protein localization as growth cones initiated a turn, cells were rapidly fixed after 12–15 min exposure to guidance cues and processed for immunocytochemistry.

*Pharmacology.* Pharmacological reagents used were thapsigargin (catalog #sc-24017A; CAS: 67526-95-8, Santa Cruz Biotechnology) 200 nM in SNM (diluted from 1 mM stock in DMSO) for 10 min to deplete ER-calcium before fixation and immunostaining; controls contained the same concentration of DMSO in the media. The membrane-permeable cyclic nucleotide Sp-cAMPS (20 $\mu$M diluted in SNM, catalog #A003S; CAS: 71774-13-5, BioLog Life Science Institute) was bath-applied 30 min before imaging.

*Imaging.* Super-resolution images were acquired using a 100/0.95 objective on a 3D-SIM microscope (OMX Blaze, DeltaVision) or on an inverted microscope (Ti2, Nikon) equipped with an Andor SRRF-Stream compatible iXon EMCCD camera. Processing of images was performed using an SRRF-Stream algorithm (Andor) and MicroManager (National Institutes of Health). Confocal images (growth cones and zebrafish larvae) were acquired using an inverted microscope (TiE, Nikon) and a laser confocal spinning disk (UltraView, PerkinElmer). Live cell imaging (all growth cone turning, optogenetic, and real-time tracking of fluorescent proteins and ER-GCaMP6 calcium imaging) was acquired using an inverted microscope (TiE, Nikon) equipped with a ×100/0.95 or 40× objective and an EMCCD camera (Photometrics). Images for EB-YFP dash movement were acquired every 7 s for 12 min; phase images were acquired every 30 s to minimize phototoxicity; hence, superimposed phase and fluorescent images do not always align perfectly. Images were acquired using NIS-Elements AR 4.00.12 software (Nikon).

*Image analysis.* Colocalized STIM1 and EB3 puncta were quantified in the peripheral zone of growth cone by first defining the area of growth cones (including filopodia), excluding the organelle-rich central zone. In super-resolution experiments, the numbers of colocalized puncta, where there was a yellow boundary between red and green puncta, illustrating likely contact, were normalized to peripheral zone area (in $\mu m^2$). To quantitate the distribution or number of microtubules, using $\beta$III-immunocytochemistry or EB3-dash dynamics, maximum intensity image projections were used to compare fluorescence on near and far sides of the growth cones (normalized to area) with respect to the micropipette. Only isolated microtubules protruding from the central zone into the periphery were assessed. All values were normalized to area before calculating near/far ratios. Microtubule trajectories/protrusions in randomly extending and turning growth cones were quantified using EB3-YFP. Images of EB-YFP-dash dynamics were acquired every 6 s for 12 min. EB3-YFP dash trajectories and velocities were measured using Manual Tracking plugin in ImageJ (National Institutes of Health). Only dashes that could be tracked for a minimum of three consecutive frames were analyzed. Dash trajectories and displacements were calculated from time-lapse movies of growth cones responding to a gradient of BDNF or sema-3a, and were presented as polar plots, which depicted the final position of EB3 dash from 3 growth cones per group. KDEL and ER-GCaMP6 fluorescence and phase-contrast images were acquired sequentially at 2 s intervals for 5 min (example shown in Movies 3, 4, 5, 6). Average change in filopodial ER-$Ca^{2+}$ ($\Delta F/F_0$) was calculated by averaging $\Delta F/F_0$ values over 20 s in sections of filopodia containing KDEL fluorescence. All image analysis was conducted using ImageJ (National Institutes of Health) or NIS Elements (Nikon).

*Light-induced activation of STIM1.* Cells were imaged in imaging buffer (SNM prepared with FluoroBrite DMEM, catalog #A1896701, Thermo Fisher Scientific). Spatially restricted regions of growth cones were stimulated with light (488 nm) using a digital mirror device (Mightex). Turning angles were calculated with ImageJ (National Institutes of Health) as the change in axon trajectory measured between the initial and final trajectories of the distal 10 $\mu$m of axons after a 12 min imaging period (2 s stimulations at 2 min and 7 min). Repulsion was defined as the angle of axon turning to the opposite side of stimulation, or a negative angle. Attraction was defined as the angle of turning toward the side of stimulation, or a positive angle. No change in turning angle was interpreted as random growth.

*Identification of zebrafish STIM1 (zSTIM1) and design of morpholino oligonucleotides. zSTIM1* (GeneID: 556360) was identified from a library of translated nucleotides using the *tblastn* tool (National Institutes of Health), with the human STIM1 sequence as a reference sequence. The zebrafish genome has two isoforms of STIM1: *zSTIM1a* and *zSTIM1b*. We chose to focus on *zSTIM1a* because it contains the STIM1-EB binding motif. From this point on, zSTIM1 refers to *zSTIM1a*. Two translation-blocking zSTIM1 morpholinos were used (#1: 5′-TCAC CAATCCGCTGAACTCCATAGT; and #2: 5′-TCAAATCCTCGCGTA GCCCGTCTCA, GeneTools) and a 5-misspaired control morpholino (5′-TCtCgAATCgGCTcAACTCCTAcT) as well as a p53 control (Gene Tools). Morpholinos (1–2 nl, at 1 mM) were injected into the yolk, exploiting cytoplasmic streaming (Bill et al., 2009) in 1–4 cell embryos.

*Dominant negative zSTIM1 plasmid design.* To generate dn-zSTIM1, a GeneString was fabricated by GeneArt (Thermo Fisher Scientific). An attB1-attB2 flanked dn-zSTIM1 construct was truncated at amino acid residue 233, and the EF-hand mutation (D70A) was included in the sequence, equivalent to the D76A previously described in human STIM1 (Liou et al., 2005; Huang et al., 2006). The Tol2 gateway system was used as described previously (Kwan et al., 2007; Don et al., 2017). Briefly, eGFP was linked at the N-terminal of zSTIM1 between amino acid residues 23 and 24. The attB1-dn-zSTIM1-eGFP-attB2 flanked construct was subcloned into pDONR-221 to make pME-dn-zSTIM1-eGFP using a Multisite Gateway BP clonase reaction. A dn-zSTIM1-GFP injection plasmid was made by combining P5E-*3mnx1* (Addgene, plasmid #74632), pME-dn-zSTIM1-eGFP and p3E-pA with pDestTol2pA2 using a Multisite Gateway Three-Fragment LR clonase reaction (Thermo Fisher Scientific) (Kwan et al., 2007). A control GFP plasmid (CTRL-GFP) was generated by replacing the pME-DN-zSTIM1-eGFP with a pME-eGFP in the above reaction. $Gal4^{s1020t}$/UAS:mCherry zebrafish embryos were injected into the single cell at the 1–2 cell stage with 50 pg of plasmid and 50 pg of transposase mRNA. Dechorionated embryos were fixed at 24 hpf with 4% PFA in PBS for 4 h at room temperature.

*Imaging and analysis of zebrafish spinal motor neuron axon pathfinding* in vivo. Axons of caudal primary (CaP) motor neurons were imaged in control, or zSTIM1 morphant $Gal4^{s1020t}$/UAS:mCherry embryos or dn-zSTIM1-GFP or CTRL-GFP axons at 20 and 24 hpf. Embryos were anesthetized in MS-222 (0.004%, catalog #E10521 CAS: 886-86-2, Sigma Aldrich) and immobilized in 1.5% agarose. Confocal stacks were acquired using 0.5 $\mu$m increments with the 525 laser line and 568 emission filter with an UltraView spinning disk confocal microscope (PerkinElmer) equipped with a ×20 objective and Volocity software (PerkinElmer). Imaging was restricted to axons of CaP motor neurons located in somites 6–10. Axon length was determined by tracing a line through the *z* projection of each CaP axon from the point of exiting the spinal cord to the distal tip of the axon. The number of filopodia were quantified by counting projections that extended $\geq$10 $\mu$m from the axon shaft in the distal 20 $\mu$m of the CaP axon. To measure the angles of axon outgrowth, brightfield images of the spinal cord, horizontal myoseptum, and ventral notochord were used as fiducial marks. Angles of axon outgrowth were measured at the exit point from the spinal cord, horizontal myoseptum, and ventral notochord. Angles >90° denoted a rostral angle of outgrowth, whereas angles <90° denoted a caudal angle of outgrowth. Quantification of CaP axon length, angles of axon outgrowth from intermediate targets, and filopodial number was performed using ImageJ (National Institutes of Health).

*Primary zebrafish spinal motor neuron culture.* Zebrafish spinal neuron cultures were generated from control or zSTIM1 morphant $Gal4^{s1020t}$/UAS:mCherry embryos. Spinal cords were isolated from embryos at 12–14 hpf and motor neurons isolated by chemical dissociation at room temperature for 10 min (in mM: as follows: 115 NaCl, 2.5 KCl, 0.4 EDTA, 8 HEPES, 0.025% trypsin, pH 7.5), triturated and plated in culture medium (Leibovitz L-15 medium supplemented with 2% FCS, Invitrogen), penicillin/streptomycin (100 $\mu$g/ml), CNTF (10 ng/ml), bFGF (500 pg/

ml), and in mM as follows: 1.25 D-glucose, 0.625 sodium pyruvate, 2.5 $CaCl_2$, 4 HEPES, pH 7.5, onto glass coverslips coated with poly-L-ornithine (1 mg/ml) and laminin (50 ng/ml). Cultures were incubated at 28°C for 4 h before all experiments.

*Calcium imaging in primary motor neuron culture.* Cells were loaded with fura-2 AM (1 $\mu$M, catalog #F1225, Invitrogen) for 10 min at room temperature in calcium-replete imaging medium (Hanks buffered saline solution, Invitrogen) supplemented with the following (in mM): 2.5 $CaCl_2$, 1 $MgCl_2$, 10 D-glucose, 15 HEPES. Fura2 images were captured every 2 s for 25 min on an inverted microscope (TiE, Nikon), using a ×40 Fluor-S oil-immersion objective equipped with DIC optics and NIS Elements 6D software (Nikon), with an attenuated illumination source (33% transmission; Lambda DG-4, Sutter Instruments). Images were acquired at 510 nm using an EMCCD digital camera (Evolve, Photometrics), in ROIs defined by NIS Elements (Nikon). To measure SOCE in cultured spinal neurons, cells were maintained in calcium-replete medium for 2 min before incubating for 5 min in calcium-deplete imaging media (Hanks buffered saline solution supplemented with the following in mM: 1 $MgCl_2$, 10 D-glucose, 15 HEPES, and 0.3 EGTA). At 7 min, thapsigargin (5 $\mu$M) was added and minimal intracellular calcium ($R_{min}$) was measured. At 17 min, calcium-replete imaging media was reintroduced. At 22 min, ionomycin (5 $\mu$M, catalog # I9657 CAS: 56092-81-0, Sigma-Aldrich) was added to induce maximal intracellular calcium ($R_{max}$). Intracellular calcium concentration was calculated in NIS elements using the following formula: $[Ca^{2+}] = K_{eff} \times (R - R_{min})/(R_{max} - R)$, where $K_{eff}$ represents the known calcium binding constant of fura-2. The magnitude of SOCE was calculated as the peak change in $[Ca^{2+}]$ following the addition of extracellular calcium.

*Imaging and analysis of calcium transients in zebrafish spinal motor neurons during axon pathfinding* in vivo. Control or zSTIM1 morphant $Gal4^{s1020t}$/UAS:GCaMP5G embryos were imaged at 16–18, 19–20, or 22–23 hpf. Embryos were paralyzed with $\alpha$-bungarotoxin (2 $\mu$M, catalog #ab120542; CAS: 11032–79-4, Abcam) and immobilized in 1.5% agarose. Calcium imaging was performed using a Carl Zeiss LSM 510 confocal imaging system equipped with HeNe laser, a water-immersion 20× W-PLAN achromatic lens, and 2.5× digital zoom. Images of CaP axons (somites 6–9) were acquired every 0.2 s for 5 min. Calcium measurements were made by defining the ROI denoting the distal axon at the relevant structures (premyoseptum, postmyoseptum, or at the myoseptum) and were measured in ImageJ (National Institutes of Health). Raw cumulative pixel intensities (fluorescence, F) were converted into changes in fluorescence from baseline ($\Delta F/F_0$) and exported to MATLAB (The MathWorks). To normalize data, minimum $\Delta F/F_0$ was corrected to 0. Calcium events were identified as peaks >2 times the SD of baseline noise, >10% of the maximum fluorescent signal, and lasting at least 0.5 s (width at half-maxima). Calcium events were categorized as low-frequency events (<7.5 events $min^{-1}$), high-frequency events (≥7.5 events $min^{-1}$), or bursting events (≥15 events $min^{-1}$) as previously described (Plazas et al., 2013).

*Zebrafish behavior.* Zebrafish larvae display a coiling behavior in response to tactile stimulation from 25 hpf that is dependent on normal axon pathfinding by CaP motor neurons (Saint-Amant and Drapeau, 1998; Nozawa et al., 2017). To assess motor activity mediated by primary motor neurons at 28 hpf, zSTIM1- or control-morphant larvae were placed in a 35 mm dish to acclimatize for at least 10 s. Larvae were stimulated using a fine needle applied to the middle of the tail. For the startle response at 52 hpf, larvae were placed into a 35 mm dish to acclimatize for at least 10 s. Larvae were stimulated using a fine needle applied dorsally approximately three-fourths along the length of the tail. Behavior was recorded using an IR-1000 Infrared CCD monochrome video camera (DAGE-MTI) on an SZX19 dissection microscope (Olympus). Recordings were captured onto a 960H Standalone DVR (Techview). A manual tracking plugin for ImageJ (National Institutes of Health) was used to quantitate movement for 10 frames following the first movement.

*Experimental design and statistical analysis.* All *in vitro* growth cone turning experiments used DRGs from 10 to 15 rats, and experiments were performed during 30–40 separate imaging sessions. Each experimental session contained at least two positive (BDNF) or negative (SNM or vehicle) controls. No more than one growth cone was imaged from each experimental dish. Operators were blinded to morpholino or siRNA treatment groups. Normality of all experimental data was assessed using D'Agostino–Pearson omnibus normality test or the Kolmogorov–Smirnov test for normality. Normally distributed data were analyzed using unpaired *t* tests with Welch's correction. Non-normal data were analyzed using Mann–Whitney *U* test or one-way ANOVA with Tukey's correction for multiple comparisons. Analyses of colocalization, filopodia and dash counts, and pixel intensity were performed using Student's *t* test, Fisher's exact test, or one-way ANOVA with Tukey's correction for multiple comparisons. Measures of ER protrusion into filopodia and numbers of filopodia-expressing KDEL were expressed as percentages, which necessitated the use of a Kruskal–Wallis test. Length and number of CaP axons were analyzed by Mann–Whitney *U* test. Cumulative frequency distributions of CaP axon outgrowth angles were analyzed by Kolmogorov–Smirnov test. Frequency and number of calcium events *in vivo* were analyzed by two-way ANOVA with Holm–Sidak test for multiple comparisons. Zebrafish behavior data were analyzed using an unpaired *t* test with Welch's correction (52 hpf data) and Mann–Whitney *U* test (24 hpf data). All scatter plots denote mean and SD. Exact *p* values are provided in the figure legends. Replicate numbers (*n*) are included in figure legends. Statistical analyses were performed using Prism 6 (GraphPad Software) or Igor Pro (Wavemetrics).

## Results

### Asymmetric activation of STIM1 is sufficient to induce growth cone turning

Asymmetric mobilization of calcium from the ER is a crucial determinant of growth cone motility in response to ER-calcium-dependent guidance cues, such as BDNF (Li et al., 2005; Mitchell et al., 2012). In contrast, cues, such as sema-3a, do not require ER-calcium release or SOCE to elicit growth cone repulsion (Song et al., 1998; Ming et al., 1999; Nishiyama et al., 2008; Mitchell et al., 2012). Hence, it was intriguing to us that STIM1 expression is necessary for netrin-1 and BDNF-induced growth cone attraction as well as sema-3a-induced growth cone repulsion (Mitchell et al., 2012; Shim et al., 2013). Given that STIM1 regulates growth cone motility in response to such diverse guidance cues, we explored the possibility that asymmetric activation of STIM1 is sufficient to steer growth cones.

To examine whether asymmetric activation of STIM1 is sufficient to activate growth cone steering, primary cultured embryonic rat (E16-E18) sensory neurons were transfected with the light-activatable STIM1 variants, OptoSTIM1 or LOVS1K (Pham et al., 2011; Kyung et al., 2015). OptoSTIM1 contains the cytosolic domain of STIM1 fused to the light-sensitive protein Cry2 and can activate SOCE, through the activation of endogenous Orai1 (Kyung et al., 2015). Spatially restricted illumination of OptoSTIM1-transfected growth cones resulted in significant turning of growth cones toward the stimulated site (Fig. 1*A–C*). This effect was not observed in growth cones expressing the light-insensitive variant, OptoSTIM1(D387A), which resulted in random growth (Fig. 1*C*). In addition to binding endogenous Orai protein at the plasma membrane to activate SOCE, the OptoSTIM1 construct retains a conserved sequence (SxIP motif at aa 642–645) enabling STIM1 binding to the microtubule EB1/EB3 (Honnappa et al., 2009). To explore whether growth cone steering in response to STIM1 activation requires interactions with microtubules, we transfected growth cones with another light-activated STIM1 variant, LOVS1K, a truncated STIM1 that contains only an Orai-activating domain (Pham et al., 2011). Significantly, growth cones transfected with LOVS1K showed variable responses to asymmetric illumination (Fig. 1*C*) that were not significantly different from those transfected with light-insensitive OptoSTIM1(D387A) (Fig. 1*C*). Furthermore, when

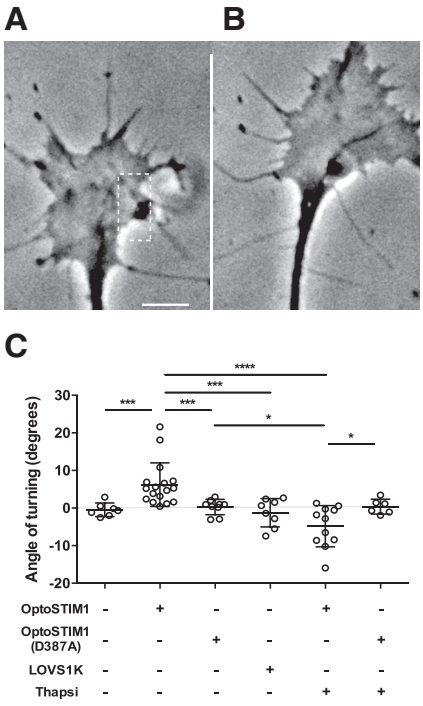


**Figure 1.** Activation of OptoSTIM1 is sufficient to steer growth cones. ***A***, ***B***, Asymmetric activation of OptoSTIM1 triggers growth cone turning toward the stimulated site. OptoSTIM1-transfected growth cone (***A***) before and (***B***) after stimulation. Dotted rectangle represents area illuminated. Image sequences were acquired for 12 min, with 2 s stimulations at 2 and 7 min. Scale bar, 5 $\mu$m. ***C***, Growth cones transfected with OptoSTIM1 ($n = 17$) turned significantly more than growth cones responding to vehicle ($n = 7$, ***$p = 0.0002$), or growth cones transfected with OptoSTIM1–D387A ($n = 9$, ***$p = 0.0002$) or LOVS1K ($n = 8$, ***$p = 0.0006$) in response to asymmetric light stimulation. Positive angles correspond to motility toward the stimulated side. Thapsigargin (thapsi) treatment abolished growth cone responses to OptoSTIM1 activation ($n = 11$, ****$p = 0.00003$), although it had no effect on turning in OptoSTIM1–D387A-transfected growth cones ($n = 6$, $p = 0.448$). Growth cones transfected with OptoSTIM1 and treated with thapsigargin turned away from the site of light activation compared with growth cones treated with OptoSTIM1–D387A (*$p = 0.017$) and OptoSTIM1–D387A+thapsi (*$p = 0.042$). Growth cones transfected and/or treated with OptoSTIM1–D387A, LOVS1K, or OptoSTIM1+thapsi were not significantly different from untransfected growth cones ($p = 0.477$, $p = 0.625$, and $p = 0.0591$, respectively). Growth cones transfected with LOVS1K did not turn significantly more than growth cones treated with OptoSTIM1–D387A ($p = 0.316$), OptoSTIM1+thapsi ($p = 0.128$), or OptoSTIM1–D387A+thapsi ($p = 0.36$) (Mann–Whitney *U* test).

thapsigargin was bath-applied to deplete the ER of calcium, turning activated by OptoSTIM1 was abolished and showed a trend toward repulsion. Thapsigargin treatment did not elicit any change in direction of turning in growth cones stimulated with the light-insensitive OptoSTIM1(D387A) (Fig. 1*C*). These data show that asymmetric activation of STIM1 is sufficient to induce growth cone turning and suggest that, in addition to activating SOCE, other STIM1 functions, such as interactions with microtubules, may also be important for the regulation of growth cone steering.

### STIM1 and EB3 are localized to microtubule plus-ends in growth cones

Microtubule end binding proteins, EB1/EB3, localize to microtubule plus-ends (Stepanova et al., 2003) to regulate the extension of microtubules into the periphery of growth cones (Geraldo et al., 2008). The close association of ER and microtubules in the growth cone periphery has been noted previously (Dailey and Bridgman, 1991; Zhang and Forscher, 2009), although ER motility during axon pathfinding and any potential underpinning of calcium regulatory mechanisms remain unexplored. We sought to examine whether the interaction of STIM1 with EB1, described previously in HeLa cells as part of a tip-associated complex to facilitate ER transport (Grigoriev et al., 2008), might be important in motile growth cones.

To examine whether STIM1 and EB colocalize to microtubules, we used super-resolution microscopy to visualize the endogenous expression of these proteins in growth cones (Fig. 2). As expected, EB3 puncta were localized to $\beta$III-tubulin-labeled microtubules, with EB3 labeling at the plus-ends of microtubules (Fig. 2*A*). Furthermore, EB3 was detected at filopodial tips, highlighting the protrusion of microtubules into distal filopodia (Fig. 2*A*,*Ci*,*Cii*, arrowheads). Similarly, STIM1 was found closely apposed with EB3 along microtubules, including in distal filopodial tips (Fig. 2*A*,*Ci*,*Cii*, arrowheads). This close association of STIM1 with EB3 at microtubule plus-ends suggests that STIM1, and therefore ER membranes, interact with EB3 proteins at growing microtubule tips.

STIM1-EB interactions are sensitive to ER-calcium concentration ($Ca^{2+}{}_{ER}$), with depletion of $Ca^{2+}{}_{ER}$ triggering dissociation of STIM1 from EB (Grigoriev et al., 2008; Asanov et al., 2013), although this can be dependent on the cell context (Tsai et al., 2014). Therefore, we asked whether depletion of $Ca^{2+}{}_{ER}$ disrupts STIM1-EB3 interactions at microtubule plus-ends in growth cones. Following treatment of cultures with 200 nM thapsigargin to chronically deplete $Ca^{2+}{}_{ER}$, we found that STIM1 and EB3 colocalization was significantly decreased in growth cones (compare Fig. 2*A* with Fig. 2*B*, and Fig. 2*Ci*,*Cii* with Fig. 2*Ciii*, quantified in Fig. 2*D*), suggesting that, when $Ca^{2+}{}_{ER}$ is depleted, STIM1 dissociates from EB3 in key areas of microtubule assembly and filopodial protrusion. These data demonstrate that STIM1 and EB3 are closely associated at plus-ends of microtubules and that this association is contingent on calcium-replete ER.

### STIM1 is required for EB3 recruitment into filopodia

The close association of STIM1 and EB3 at microtubules suggests that STIM1 is coupled, or tethered, to microtubules in growth cones. We therefore reasoned that STIM1 could regulate microtubule motility in growth cones. To examine this, we treated DRG neurons with a control (STIM1-CTRL) or STIM1-specific morpholino (STIM1-KD) to reduce STIM1 expression. To assess knockdown, we measured STIM1 immunoreactivity across growth cones as integrated density (intensity/$\mu m^2$, arbitrary units) and found a significant reduction in STIM1 expression (mean 0.064 $\pm$ 0.004 A.U.; $n = 26$) compared with controls (mean 0.19 $\pm$ 0.1 A.U.; $n = 21$; $p = 5.5E\text{-}06$, Mann–Whitney *U* test), which was consistent with our previous work (Gasperini et al., 2009; Mitchell et al., 2012). We simultaneously transfected neurons with a morpholino and EB3-YFP (Stepanova et al., 2003; Geraldo et al., 2008) to visualize microtubule tip dynamics. EB3 dashes (or "comets") demarcate microtubule plus-end polymerization and can be used to define the trajectory and velocity of microtubule growth (Stepanova et al., 2003). While EB3 dashes were evident in STIM1-CTRL and STIM1-KD growth cones, there was a clear difference in EB3 spatiotemporal dynamics (compare Movie 1 with Movie 2). In STIM1-CTRL growth cones, EB3 dashes were abundant in both central and peripheral domains (Movie 1; Fig. 2*E*), whereas EB3 dashes were restricted predominantly to the central domain in STIM1-KD growth cones (Movie 2; Fig. 2*F*). Examination of dash velocities revealed that microtubules protruded more slowly after

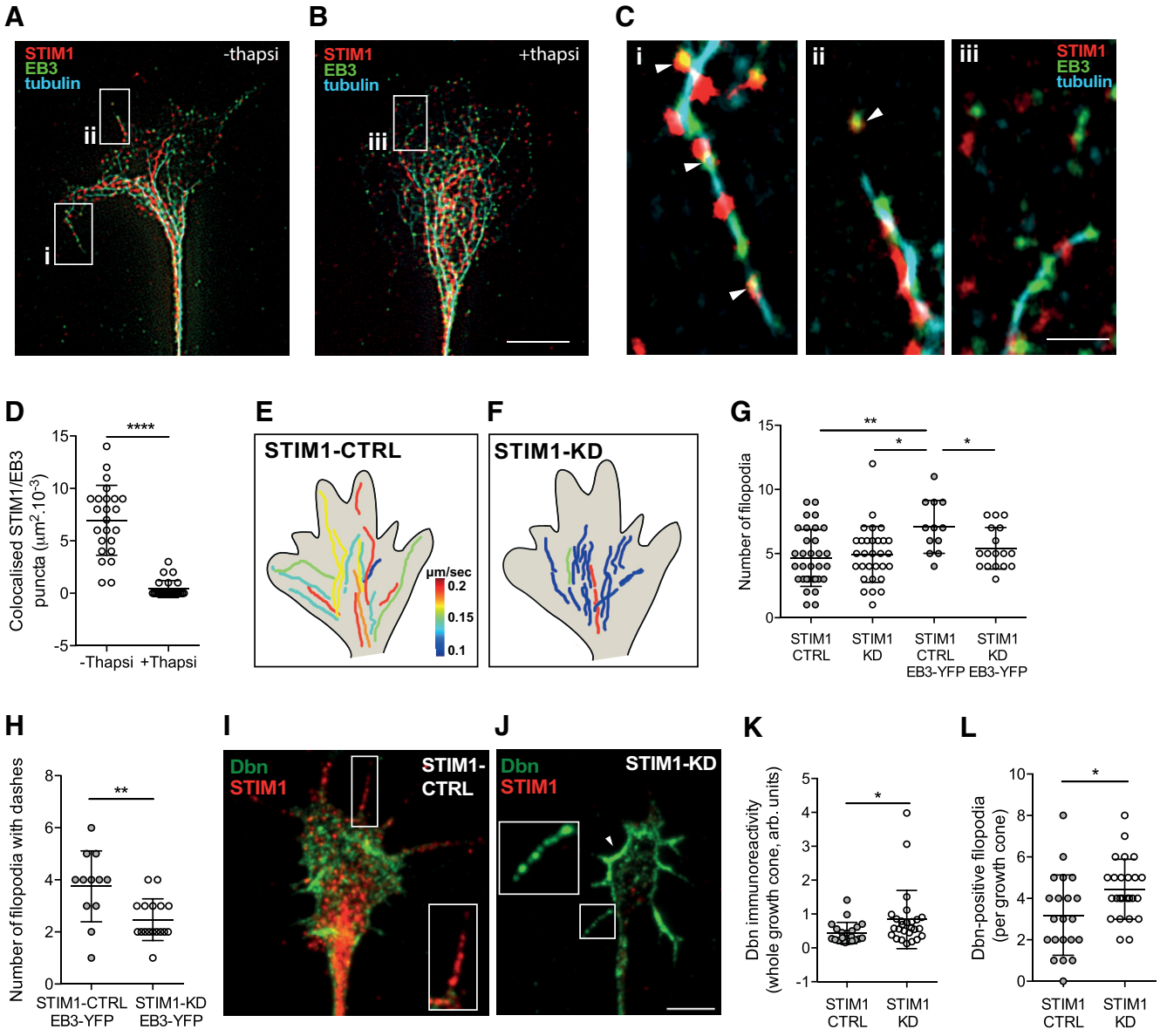


**Figure 2.** STIM1 regulates microtubule tip dynamics at the periphery of sensory growth cones. ***A–C***, Super-resolution images of growth cones in the absence or presence of the SERCA inhibitor, thapsigargin (200 nM for 10 min) and immunostained for β-III tubulin (cyan), STIM1 (red), or EB3 (green) protein. STIM1 colocalizes with EB3 proteins and microtubules with STIM1/EB3 puncta detected on microtubules in filopodia (***A***, arrowheads in insets ***i*** and ***ii*** shown in ***Ci*** and ***Cii***, respectively). When growth cones were treated with thapsigargin (***B***), there was uncoupling of STIM1 and EB3 puncta on microtubules in the peripheral (transition) zone of growth cones (***B***, inset ***iii*** shown in ***Ciii***). ***D***, Colocalization of STIM1/EB3 was greater in the periphery of growth cones in controls ($n = 25$) compared with growth cones treated with thapsigargin ($n = 24$, $^{****}p = 8.9E\text{-}10$, Mann–Whitney *U* test). Scale bars: ***A***, ***B***, 5 μm; ***C***, 1 μm. ***E***, ***F***, Microtubule tip dynamics were examined in STIM1-CTRL and STIM1-KD growth cones transfected with EB3-YFP. Composite representation of EB3-YFP dash trajectories in (***E***) STIM1-CTRL and (***F***) STIM1-KD growth cones, pseudo-colored for dash velocity (μm/s), comprising 5–7 dashes from each of 3 STIM1-CTRL and STIM1-KD growth cones (see also Movies 1, 2; Table 1). Heat map in ***E*** represents EB3-dash velocity. ***G***, Total number of filopodia in STIM1-CTRL was greater after EB3-YFP overexpression ($n = 12$) compared with STIM1-CTRL alone ($n = 32$, $^{**}p = 0.002$) or STIM1-KD ($n = 30$, $^{*}p = 0.006$) or STIM1-KD EB3-YFP ($n = 17$, $^{*}p = 0.0215$). The number of filopodia was not significantly different between STIM1-CTRL growth cones and STIM1-KD ($p = 0.621$) or STIM1-KD EB3-YFP ($p = 0.221$), and there was no difference between STIM1-KD and STIM1-KD EB3-YFP ($p = 0.435$, one-way ANOVA, Tukey's multiple comparison test). ***H***, The number of filopodia with EB3 dashes was reduced in STIM1-KD ($n = 17$) compared with STIM1-CTRL growth cones ($n = 12$, $^{**}p = 0.0036$, Student's *t* test). ***I***, STIM1-CTRL and (***J***) STIM1-KD growth cones immunolabeled with drebrin (green) and STIM1 (red). Arrowheads indicate significant drebrin expression at lamellipodial border. Scale bar, 5 μm. ***K***, Drebrin immunoreactivity was increased across whole growth cones after STIM1-KD ($n = 25$) compared with STIM1-CTRL ($n = 21$, $^{*}p = 0.016$, Mann–Whitney *U* test). ***L***, Drebrin expression in filopodia was inversely correlated to STIM1 expression. The number of filopodia immunoreactive for drebrin was increased after STIM1-KD ($n = 25$) compared with STIM1-CTRL ($n = 21$, $^{*}p = 0.0162$, Student's *t* test).

STIM1-KD treatment compared with STIM1-CTRL growth cones (Fig. 2*E*,*F*; Table 1).

Given the importance of microtubule extension into filopodia during growth cone steering (Tanaka and Kirschner, 1995; Dent et al., 1999; Gallo and Letourneau, 1998, 1999), we next asked whether STIM1 was required for EB3 dash recruitment to filopodia and whether filopodial number was altered by STIM1 expression. STIM1-CTRL and STIM1-KD growth cones had comparable numbers of filopodia (Fig. 2*G*); and not unexpectedly, the number of filopodia in STIM1-CTRL growth cones transfected with EB3-YFP was increased (Fig. 2*G*), most likely through enhanced recruitment of +TIP effectors, such as drebrin (Geraldo et al., 2008). Interestingly, the knockdown of STIM1 expression abolished this EB3-mediated increase in filopodia number (Fig. 2*G*), highlighting the interplay between STIM1 and EB3. We found that filopodia in STIM1-KD growth cones were

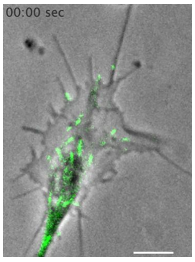


**Movie 1.** EB3-YFP illustrates dynamic microtubule tip movement throughout a STIM1-CTRL growth cone. Time lapse sequence of randomly extending, STIM1-CTRL growth cone transfected with EB3-YFP (green dashes) to illustrate microtubule movement. EB3 dashes can be observed moving from the center of the growth cone out to the periphery. Movies are shown in real time with seconds displayed. Scale bar, 5 $\mu$m.

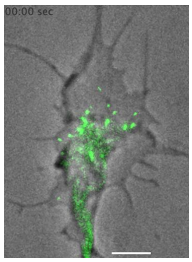


**Movie 2.** EB3-YFP illustrates perturbed microtubule tip dynamics in a STIM1-KD growth cone. Time lapse sequence of randomly extending, STIM1-KD growth cone transfected with EB3-YFP (green dashes) to illustrate microtubule movement. EB3 dashes appear to be restricted predominantly to the central domain in STIM1-KD growth cones. Movies are shown in real time with seconds displayed. Scale bar, 5 $\mu$m.

**Table 1. STIM1 knockdown disrupts EB3 comet-like dash dynamics[a]**

| | STIM1-CTRL | STIM1-KD |
|---|---|---|
| Average dash number per frame[b] in growth cone | 0.031 ± 0.0131 | 0.018 ± 0.0130 |
| Average dash velocity[c] in growth cone | 0.17 ± 0.07 | 0.11 ± 0.04* |
| Average distance[d] per dash ($\mu$m) in growth cone | 1.07 ± 0.36 | 0.71 ± 0.26** |
| Average track length ($\mu$m) in growth cone | 9 ± 5.85 | 3.81 ± 1.58*** |
| Average filopodial dash velocity[c] | 0.37 ± 0.13 | 0.29 ± 0.05**** |

[a]Microtubule dynamics were examined by overexpressing EB3-YFP in STIM1-CTRL and STIM1-KD growth cones. Dash velocity, distance, and track length in whole growth cone were analyzed in 6 dashes of STIM1-CTRL (54 in 9 separate growth cones) and STIM1-KD (36 in 6 separate growth cones) growth cones. Filopodial EB-dash velocity was analyzed in single filopodia from STIM1-CTRL (12) and STIM1-KD (13) growth cones expressing EB3-YFP.

[b]Images acquired every 6 s. Number of dashes per frame were normalized to growth cone area.

[c]Values are $\mu$m/s ± SD.

[d]Value calculated from average of distance traveled by a single dash per frame.

*$p = 0.000006$; **$p = 0.0000015$; ***$p = 0.0000013$; ****$p = 0.036$.

less likely to contain EB3 dashes (Fig. 2*H*); and as described above, when present, EB3 dashes protruded more slowly than EB3 dashes in STIM1-CTRL growth cones (Fig. 2*E*,*F*; Movies 1, 2; Table 1). These data suggest that STIM1 regulates EB3 dynamics and hence microtubule extension into the periphery of growth cones.

The persistence of filopodia in STIM1-KD growth cones, despite the apparent disruption to EB3 dynamics, suggested that compensatory mechanisms are activated to maintain filopodia. We therefore asked whether the expression of drebrin, a regulator of filopodial initiation (Geraldo et al., 2008), was altered in STIM1-KD growth cones. We detected prominent drebrin expression in the peripheral zone of STIM1-CTRL growth cones, although not in all filopodia (Fig. 2*I*, inset, *K*,*L*). In contrast, significantly higher drebrin expression was observed in STIM1-KD growth cones (Fig. 2*J*, inset, *K*,*L*), especially at the growth cone leading edge, along lamellipodial borders and in filopodia (Fig. 2*J*, inset and arrowhead, *K*,*L*). These data suggest that a reduction of STIM1 expression causes drebrin to be upregulated to support growth cone motility.

### STIM1 is required for ER remodeling into filopodia

STIM1-EB interactions at microtubule plus-ends suggest a potential mechanism to facilitate remodeling of the ER in growth cones, particularly into peripheral filopodia to localize calcium signaling. To visualize the dynamics of ER and microtubule tips in filopodia, we cotransfected neurons with BiP-mCherry-KDEL to label ER membranes (Zurek et al., 2011) and EB3-YFP (Fig. 3*A–F*; Movies 3, 4, 5, 6). We observed significant protrusion of EB3 signal with associated ER cargo, into filopodia of STIM1-CTRL growth cones (Fig. 3*A*,*Ci*,*Cii*,*E*; Movies 3, 4). In STIM1-KD growth cones, there was no difference in the number of filopodia containing ER (Fig. 3*B*,*Di*,*Dii*,*E*; Movies 5, 6); however, in the STIM1-KD filopodia that did contain ER, the distance that microtubules and associated ER protruded into the filopodia was significantly reduced (Fig. 3*F*), demonstrating that ER translocates more slowly when STIM1 expression is reduced (compare Fig. 3*Cii* with Fig. 3*Dii*; Movies 4, 6; Table 1). These data are striking, given that there is only a partial reduction of STIM1 expression, suggesting that a threshold level of STIM1 expression is required for STIM1 to function effectively to regulate ER remodeling and protrusion into growth cone filopodia.

Because STIM1 is known to be crucial in regulating $Ca^{2+}_{ER}$ levels, we next examined STIM1 regulation of $Ca^{2+}_{ER}$ within filopodia. To report filopodial $Ca^{2+}_{ER}$, we cotransfected neurons with a genetically encoded $Ca^{2+}_{ER}$ sensor, ER-GCaMP6 (de Juan-Sanz et al., 2017) and EB3-tdTomato (Fig. 3*G*,*H*). In STIM1-CTRL growth cones, the $Ca^{2+}_{ER}$ signal within filopodia closely followed the EB3 signal (Fig. 3*G*). Notably, elevated $Ca^{2+}_{ER}$ signals were evident at or near EB3 at the microtubule tips in STIM1-CTRL filopodia (Fig. 3*Gii*, arrowheads), that may indicate sites of ER refilling. Sites of reduced ER-GCaMP6 signals, possibly indicating areas of ER emptying, were also detected in STIM1-CTRL filopodia (Fig. 3*Gi*, asterisks). In STIM1-KD growth cones, the $Ca^{2+}_{ER}$ signal within filopodia was dramatically reduced; and focal $Ca^{2+}_{ER}$ intensities, potential sites of ER filling, were rarely seen (Fig. 3*Hi*,*Hii*).

To further explore the potential for $Ca^{2+}_{ER}$ refilling and emptying in filopodia, growth cones were cotransfected with both the ER-GCaMP6 and the BiP-mCherry-KDEL plasmids (Fig. 3*I–M*; Movies 7, 8). There was extensive overlap between the expression patterns of the ER membranes and calcium signals in filopodia of STIM1-CTRL growth cones (Fig. 3*I*,*Ki*,*Kii*,*M*; Movie 7), which was predicted given that both constructs use a KDEL localization sequence. In STIM1-CTRL filopodia, we observed distinct regions where the GCaMP6 and BiP-mCherry-KDEL signals overlapped, denoting $Ca^{2+}$-replete ER (Fig. 3*Kii*), as well as regions where BiP-mCherry-KDEL was observed alone, highlighting areas of $Ca^{2+}_{ER}$ depletion (Fig. 3*Kii*). This pattern of $Ca^{2+}_{ER}$ depletion and refilling was observed in STIM1-CTRL filopodia as alternating regions of BiP-mCherry-KDEL alone or colocalized BiP-mCherry-KDEL and GCaMP6 signals (Fig. 3*Ki*,*Kii*). Significantly, in STIM1-KD filopodia, $Ca^{2+}_{ER}$ was dramatically reduced, such that $Ca^{2+}_{ER}$ signals were barely detectable (Fig. 3*J*,*Li*,*Lii*,*M*; Movie 8). The reduction of filopodial $Ca^{2+}_{ER}$ after

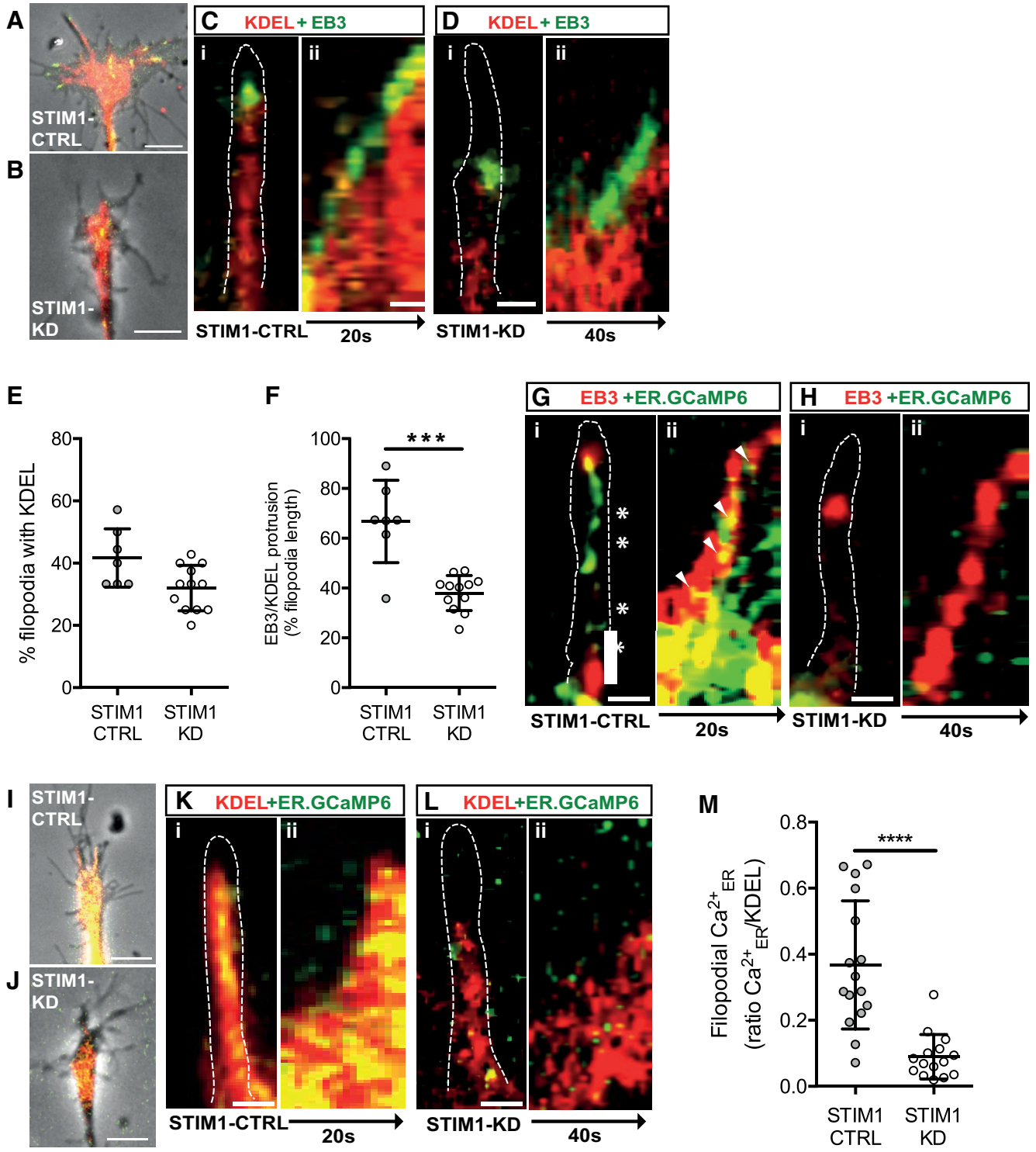


**Figure 3.** STIM1 is required for microtubule-ER remodeling and calcium signals in filopodia. ***A–F***, STIM1-CTRL and STIM1-KD neurons were cotransfected with BiP-mCherry-KDEL (ER membrane marker) and EB3-YFP. Images of (***A***) STIM1-CTRL and (***B***) STIM1-KD growth cones expressing KDEL (red) and EB3 (green). Scale bar, 5 $\mu$m. ***Ci***, ***Di***, KDEL and EB3 localization in single filopodia (outlined). ***Cii***, ***Dii***, Representative kymographs of KDEL (red) and EB3 (green) protrusion into STIM1-CTRL (***C***) and STIM1-KD (***D***) filopodia, displayed over 20 and 40 s, respectively. Scale bars, 500 nm. ***E***, The percentage of filopodia with a KDEL signal in STIM1-CTRL filopodia ($n = 7$) was not significantly different from STIM1-KD filopodia ($n = 12$) ($p = 0.0224$, Kruskal–Wallis test). ***F***, The distance EB3 dashes with KDEL signals protruded into filopodia was significantly reduced in STIM1-KD compared with STIM1-CTRL filopodia (***$p = 0.003$, Kruskal–Wallis test, see Movies 3, 4, 5, 6). ***G***, ***H***, STIM1-CTRL ($n = 12$) and STIM1-KD ($n = 16$) sensory neurons were cotransfected with ER-GCaMP6 –150 ($Ca^{2+}_{ER}$ reporter) and EB3-tdTomato. ***Gi***, ***Hi***, ER-GCaMP6 (green) and EB3 (red) in filopodia (outlined). ***Gii***, ***Hii***, Representative kymographs of ER-GCaMP6 (green) and EB3 (red) protrusion into STIM1-CTRL (***Gii***) and STIM1-KD (***Hii***) filopodia, displayed over 20 and 40 s, respectively. Scale bars, 500 nm. ***I–M***, STIM1-CTRL and STIM1-KD sensory neurons were cotransfected with BiP-mCherry-KDEL and ER-GCaMP6. Images of (***I***) STIM1-CTRL and (***J***) STIM1-KD growth cones expressing KDEL (red) and ER-GCaMP6 (green). Scale bar, 5 $\mu$m. ***Ki***, ***Li***, ER-GCaMP6 (green) and KDEL (red) in filopodia (outlined). ***Kii***, ***Lii***, Representative kymographs of ER-GCaMP6 (green) and KDEL (red) as ER membrane extends into STIM1-CTRL(***Kii***) and STIM1-KD (***Lii***) filopodia, displayed over 20 and 40 s, respectively. Scale bar, 500 nm. ***M***, The filopodial ER-GCaMP6 signal, $\Delta F/F$ normalized to KDEL signal, and averaged over 20 s was significantly reduced in STIM1-KD ($n = 15$) compared with STIM1-CTRL filopodia ($n = 16$, ****$p = 0.00003$, Student's *t* test, see Movies 7, 8).

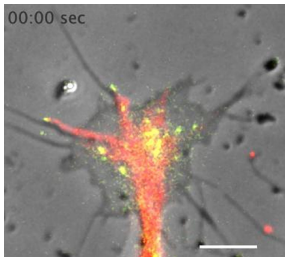


**Movie 3.** Microtubule tips lead ER remodeling into the periphery of a STIM1-CTRL growth cone. Time lapse sequence of a randomly extending, STIM1-CTRL growth cone transfected with EB3-YFP (green) and BiP-mCherry-KDEL (red) to illustrate microtubule and ER movement, respectively. Significant protrusion of the EB3 signal with associated ER cargo can be observed throughout the STIM1-CTRL growth cone and along the full length of several filopodia. Movies are shown in real time with seconds displayed. Scale bar, 5 $\mu$m.

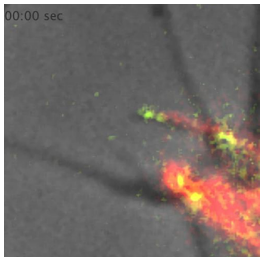


**Movie 4.** Microtubule tips lead ER remodeling into STIM1-CTRL filopodia. Time lapse sequence of STIM1-CTRL filopodia, transfected with EB3-YFP (green) and BiP-mCherry-KDEL (red) to illustrate microtubule and ER movement, respectively. Significant protrusion of the EB3 signal with associated ER cargo can be observed moving along almost the entire length of filopodia. Movies are shown in real time with seconds displayed. Scale bar, 5 $\mu$m.

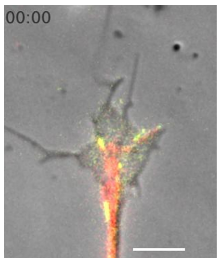


**Movie 5.** Microtubule tips and ER remodeling are largely confined to the central zone of a STIM1-KD growth cone. Time lapse sequence of randomly extending, STIM1-KD growth cone transfected with EB3-YFP (green) and BiP-mCherry-KDEL (red) to illustrate microtubule and ER movement, respectively. Protrusion of the EB3 signal with associated ER cargo appears largely confined to the central zone of the STIM1-KD growth cone, with limited protrusion of microtubule tips and associated ER along the length of the filopodia. Movies are shown in real time with seconds displayed. Scale bar, 5 $\mu$m.

STIM1 knockdown was highlighted by measuring total filopodial $Ca^{2+}_{ER}$, normalized to the total KDEL signal over time. We observed a significant decrease in $Ca^{2+}_{ER}$ in STIM1-KD compared with the $Ca^{2+}_{ER}$ signals detected in STIM1-CTRL cells (Fig. 3*M*). These data demonstrate a requirement for STIM1 in the protrusion of ER into the filopodia as well as the calcium content of the filopodial ER.

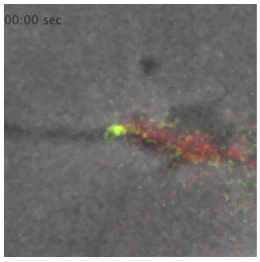


**Movie 6.** STIM-KD reduced the protrusion of microtubule tips and ER into filopodia. Time lapse sequence of STIM1-KD filopodia, transfected with EB3-YFP (green) and BiP-mCherry-KDEL (red) to illustrate microtubule and ER movement, respectively. There was limited protrusion of the EB3 signal with associated ER cargo along the filopodia. Movies are shown in real time with seconds displayed. Scale bar, 5 $\mu$m.

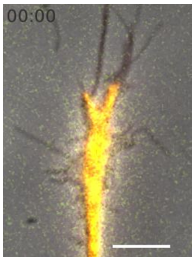


**Movie 7.** Robust $Ca^{2+}_{ER}$ signals throughout the ER in a STIM-CTRL growth cone. Time lapse sequence of STIM1-CTRL growth cone, transfected with ER-GCaMP6 (green) and BiP-mCherry-KDEL (red). There was extensive overlap between the ER membranes and calcium signals throughout the STIM1-CTRL growth cones. Furthermore, the $Ca^{2+}_{ER}$ signal fluctuated over time indicating the emptying and refilling of calcium stores. Movies are shown in real time with seconds displayed. Scale bar, 5 $\mu$m.

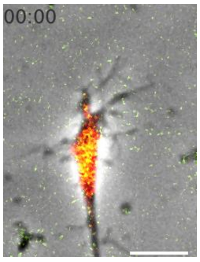


**Movie 8.** $Ca^{2+}_{ER}$ signals are reduced in the ER in a STIM-KD growth cone. Time lapse sequence of STIM1-KD growth cone, transfected with ER-GCaMP6 (green) and BiP-mCherry-KDEL (red). While some $Ca^{2+}_{ER}$ signal was detected, overlapping with the ER membranes, it was greatly reduced after STIM1-KD. Movies are shown in real time with seconds displayed. Scale bar, 5 $\mu$m.

### STIM1 is required for recruitment of EB to the motile side of steering growth cones

Growth cone steering is underpinned by the transduction of guidance cues leading to asymmetric microtubule stabilization and protrusion into peripheral areas of growth cones (Williamson et al., 1996; Buck and Zheng, 2002). We have previously

shown that STIM1 is actively translocated to the "turning" side of growth cones during steering (Mitchell et al., 2012), but exactly how this spatial reorganization is regulated and the functional consequences of STIM1 translocation during steering is not known. Significantly, EB proteins promote microtubule extension and protrusion in growth cones (Geraldo et al., 2008), and our data demonstrate that STIM1 regulates EB3 motility in the peripheral domains of growth cones, including filopodia. Therefore, we next asked whether STIM1 is required for microtubule recruitment to the motile side of actively steering growth cones.

We exposed STIM1-CTRL and STIM1-KD growth cones to pulsatile microgradients of the ER-calcium-dependent, attractive guidance cue BDNF or the ER-calcium-independent, repulsive guidance cue sema-3a (Fig. 4) and measured EB3 dash motility in "near" and "far" regions (illustrated in Fig. 4*I*, inset) of growth cones as they turned toward or away from guidance cues. The trajectories and velocities (color-coded, $\mu$m/s) of EB3 dashes within isolated growth cones (Fig. 4*A–D*) turning toward BDNF and away from sema-3a suggest that reducing STIM1 expression slows EB3 dash velocity and disrupts the localization of EB3 away from the turning side of the growth cone. This observation was borne out over multiple growth cones, where analysis of EB3 dash trajectories in STIM1-CTRL growth cones exposed to BDNF revealed that EB3 translocated to the motile or "near" side of growth cones (Fig. 4*A*,*E*; Movie 9; quantified in Fig. 4*I*). Crucially, reducing STIM1 expression not only abolished the recruitment of EB3 to the "near" side of growth cones exposed to BDNF, but switched EB3 dash localization to the "far" side (Fig. 4*B*,*F*; Movie 10; quantified in Fig. 4*I*). These findings are consistent with a switch from attractive to repulsive turning in STIM1-KD growth cones turning in response to BDNF (Mitchell et al., 2012). When STIM1-CTRL growth cones were exposed to sema-3a, they were repelled and EB3 dashes again translocated to the motile (in this case the "far" side) of the growth cone (Fig. 4*C*,*G*; Movie 11; quantified in Fig. 4*I*). However, when STIM1-KD growth cones were exposed to sema-3a, EB3 recruitment to the "far" side was abolished and a random distribution of EB3 dashes was observed (Fig. 4*D*,*H*; Movie 12; quantified in Fig. 4*I*), consistent with our previous data showing that STIM1 reduction caused random steering in response to sema-3a (Mitchell et al.,

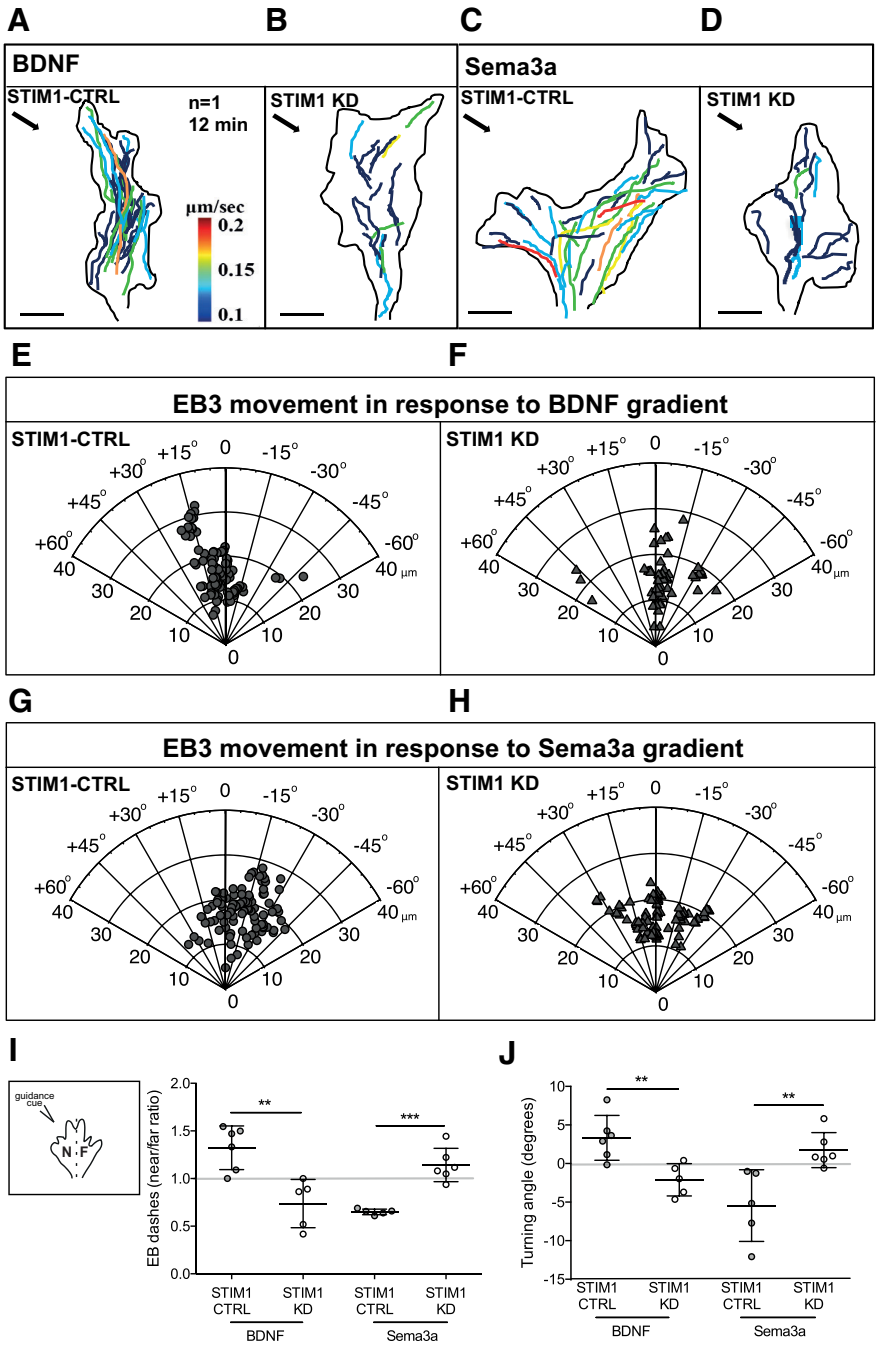


**Figure 4.** STIM1 regulates EB3-YFP recruitment to the motile side of turning growth cones. ***A–D***, Maximum intensity projections of EB3 dash trajectories in representative STIM1-CTRL and STIM1-KD growth cones turning to (***A***,***B***) BDNF and (***C***,***D***) sema-3a (gradient direction demarcated by arrow in top-left corner). EB3-labeled tracks quantified in time over 12 min (color-coded for average velocity per dash, $\mu$m/s). ***E–H***, Polar plots depicting EB3 dash displacement and trajectories in STIM1-CTRL ($n = 3$; ***E***,***G***) and STIM1-KD ($n = 6$; ***F***,***H***) growth cones turning in response to a gradient of (***E***,***F***) BDNF or (***G***,***H***) sema-3a. Positive angles represent attraction and negative angles represent repulsion with respect to the initial trajectory of the growth cone. ***I***, Near/far ratio of all EB3-YFP dashes in STIM1-CTRL ($n = 6$) and STIM1-KD ($n = 5$) growth cones exposed to BDNF or sema-3a gradients ($n =$ 5 STIM1-CTRL and $n = 6$ STIM1-KD). The final EB3 positions switched from near to far in growth cones turning in response to BDNF after STIM1 knockdown (**$p = 0.0033$). The final EB3 positions switched from far to a random distribution in growth cones turning in response to sema-3a after STIM1 knockdown (***$p = 0.0002$, one-way ANOVA, Tukey's multiple comparison test). Inset, Schematic illustrating definition of near (N) and far (F) side of the growth cone with respect to the source of guidance cue (see Movies 9, 10, 11, 12). ***J***, Average turning angles of STIM1-CTRL and STIM1-KD growth cones exposed to BDNF or sema-3a gradients for 12 min (datasets include all growth cones depicted in ***A–H***). Turning angles switched from attraction to repulsion in growth cones turning to BDNF after STIM1 knockdown (**$p = 0.006$), and from repulsion to random growth in response to sema-3a (**$p = 0.008$, one-way ANOVA, Tukey's multiple comparison test).

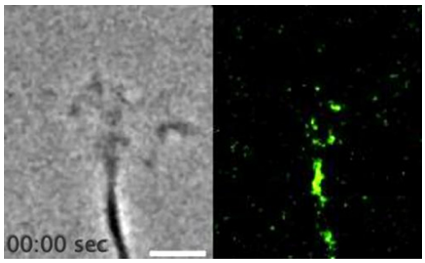


**Movie 9.** Microtubule tips translocate to the near side of a STIM-CTRL growth cone turning toward a source of BDNF. Time lapse sequence of a STIM1-CTRL growth cone (phase image left), transfected with EB3-YFP (green, right image), turning toward a source of BDNF (top left quadrant, out of FOV). As the growth cone orients toward the source of BDNF, the microtubule tips also track toward the near side of the growth cone. Colored lines on fluorescent movies indicate tracks of individual EB3-YFP puncta. The BDNF gradient begins at the start of the movie. Movies are shown in real time with seconds displayed. Scale bar, 5 $\mu$m.

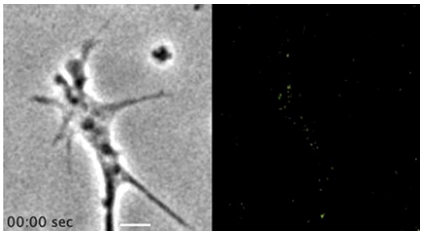


**Movie 10.** Microtubule tips translocate to the far side of a STIM-KD growth cone turning away from a source of BDNF. Time lapse sequence of a STIM1-KD growth cone (phase image left), transfected with EB3-YFP (green, right image), turning away from a source of BDNF (top left quadrant, out of FOV). As the growth cone orients away from the source of BDNF, the microtubule tips track toward the far side of the growth cone. Colored lines on fluorescent movies indicate tracks of individual EB3-YFP puncta. The BDNF gradient begins at the start of the movie. Movies are shown in real time with seconds displayed. Scale bar, 5 $\mu$m.

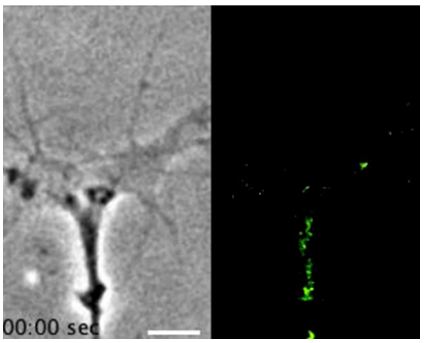


**Movie 11.** Microtubule tips translocate to the far side of a STIM-CTRL growth cone turning away from a source of sema-3a. Time lapse sequence of a STIM1-CTRL growth cone (phase image left), transfected with EB3-YFP (green, right image), turning away from a source of sema-3a (top left quadrant, out of FOV). As the growth cone turns away from the source of sema-3a, the microtubule tips track toward the far side of the growth cone. Colored lines on fluorescent movies indicate tracks of individual EB3-YFP puncta. The sema-3a gradient begins at the start of the movie. Movies are shown in real time with seconds displayed. Scale bar, 5 $\mu$m.

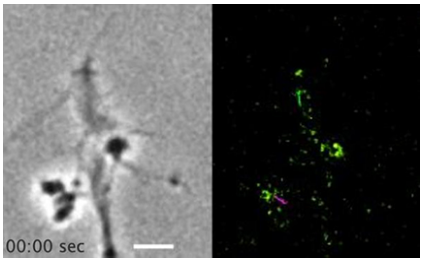


**Movie 12.** Microtubule tips translocate to the far side of a STIM-KD growth cone that fails to turn away from a source of sema-3a. Time lapse sequence of a STIM1-KD growth cone (phase image left), transfected with EB3-YFP (green, right image), that fails to turn in response to a source of sema-3a (top left quadrant, out of FOV). The growth cone grows randomly, despite the source of sema-3a; and similarly, the trajectories of the microtubule tips are random, not biased to the near or far side of the growth cone. Colored lines on fluorescent movies indicate tracks of individual EB3-YFP puncta. The sema-3a gradient begins at the start of the movie. Movies are shown in real time with seconds displayed. Scale bar, 5 $\mu$m.

2012). The angle of growth cone turning in response to BDNF and sema-3a is shown in Figure 4*J*, and is consistent with that described previously after STIM1 knockdown (Mitchell et al., 2012). These data suggest that STIM1 regulates microtubule dynamics in response to ER-calcium-dependent and -independent guidance cues and that STIM1 is necessary for the asymmetric microtubule protrusion that directs growth cone motility in response to guidance cues *in vitro*.

### STIM1 is required for the spatial recruitment of microtubules to the motile side of steering growth cones

As STIM1 was necessary for the recruitment of EB3 to the motile side of steering growth cones, we sought to confirm that STIM1 does regulate microtubule recruitment. We first examined the spatial distribution and number of microtubules in growth cones during random growth (Fig. 5*A–E*). STIM1-KD growth cones showed significantly fewer microtubules compared with STIM1-CTRL growth cones (compare Fig. 5*A*,*B*, quantified in Fig. 5*D*). Importantly, total $\beta$III-tubulin expression across the entire growth cone was unaffected by reduced STIM1 expression (Fig. 5*E*). Knockdown of Orai1 had no significant effect on microtubule number in randomly extending growth cones (Fig. 5*C–E*), consistent with SOCE occurring downstream of STIM1-microtubule interactions (Asanov et al., 2013; Chang et al., 2018).

We next sought to confirm whether STIM1 facilitates the preferential localization of microtubules to the motile side of steering growth cones. STIM1-CTRL and STIM1-KD growth cones were exposed to micro-gradients of BDNF or sema-3a for 15 min before being fixed and immunostained to detect $\beta$III-tubulin. In STIM1-CTRL growth cones exposed to BDNF, the number of microtubules was significantly biased toward the motile or "near" side of the growth cone (Fig. 5*F*). Similarly, in STIM1-CTRL growth cones exposed to sema-3a, microtubules occupied the motile side of the growth cone; in this case, the "far" side (Fig. 5*F*). However, in STIM1-KD growth cones, the spatial recruitment of microtubules to the "near" side was lost, such that in response to BDNF, microtubules were located to the "far" side and similarly, in response to sema-3a, microtubule recruitment was abolished, consistent with random growth (Fig. 5*F*). These data confirm the requirement of STIM1-EB3 interactions for microtubule recruitment to the motile side of steering growth cones,

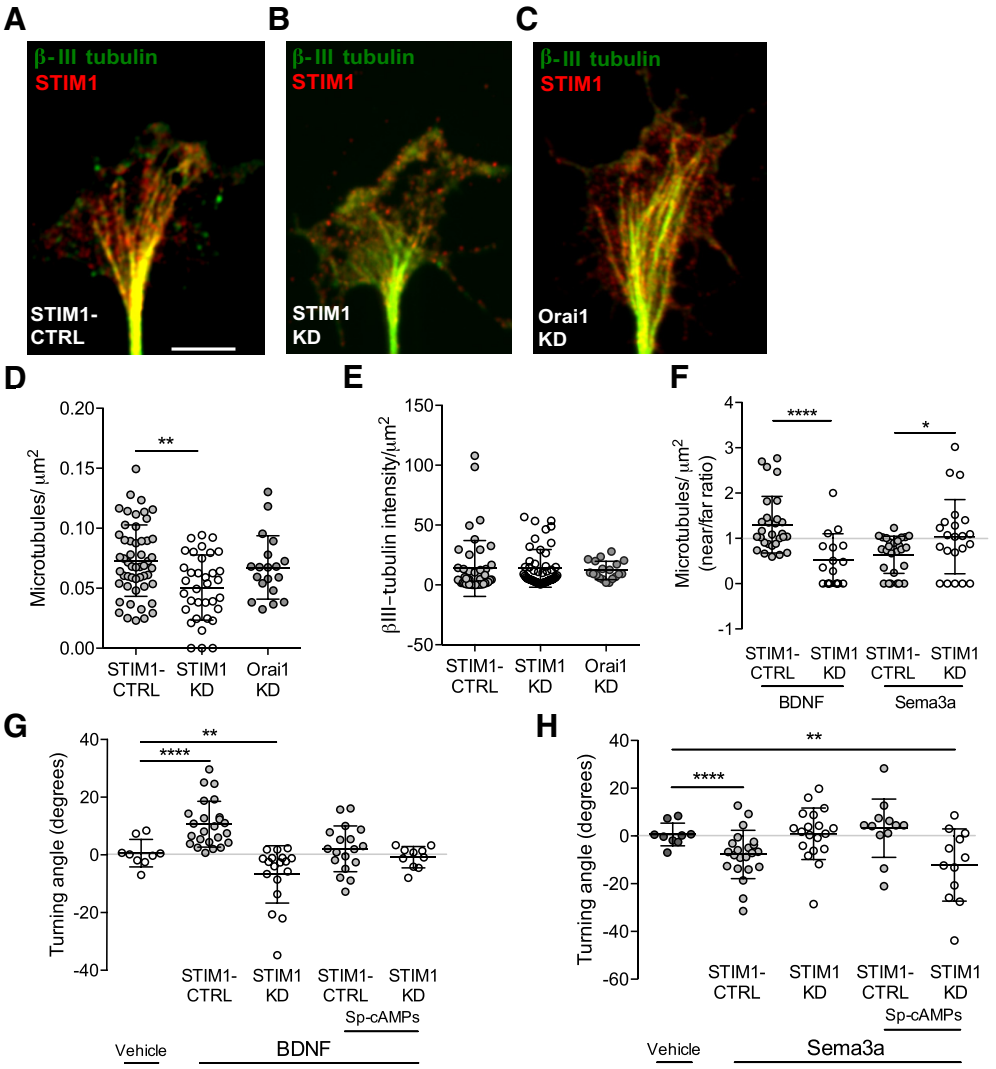


**Figure 5.** STIM1 is necessary for microtubule recruitment during growth cone steering. ***A–C***, Images of (***A***) STIM1-CTRL, (***B***) STIM1-KD, and (***C***) Orai1-KD growth cones immunostained for β-III tubulin (green) and STIM1 (red). Scale bar, 5 μm. ***D***, The number of microtubules (normalized to growth cone area) was reduced in STIM1-KD ($n = 35$) growth cones compared with STIM1-CTRL ($n = 46$, $^{**}p = 0.006$), but not different after Orai1-KD ($n = 21$, $p = 0.46$, one-way ANOVA, Tukey's multiple comparison test). ***E***, Total β-III tubulin immunoreactivity measured by integrated density was not different between STIM1-CTRL, STIM1-KD ($p = 0.991$), or Orai1-KD growth cones ($p = 0.756$, one-way ANOVA, Tukey's multiple comparison test). ***F***, Near/far ratio of microtubules (normalized to growth cone area) in STIM1-CTRL and STIM1-KD growth cones exposed to BDNF or sema-3a gradients. The distribution of microtubules switched from near (STIM1-CTRL, $n = 31$) to far (STIM1-KD, $n = 17$) in growth cones turning in response to BDNF ($^{****}p = 0.0001$). The distribution of microtubules switched from far (STIM1-CTRL, $n = 33$) to random distribution (STIM1-KD, $n = 22$) in growth cones turning in response to sema-3a ($^{*}p = 0.0322$, Student's *t* test). ***G***, Growth cone turning in response to BDNF after STIM1-KD could not be restored by manipulating cAMP signaling (all turning is compared with vehicle, random growth, $n = 23$). STIM1-CTRL growth cones turned toward a source of BDNF ($n = 24$, $^{****}p = 0.000005$), while turning toward BDNF was abolished by activation of PKA with bath application of Sp-cAMPs ($n = 18$, $p = 0.49$ from vehicle, $^{**}p = 0.0018$ from STIM1-CTRL). STIM1-KD growth cones turned away from BDNF ($n = 18$, $^{**}p = 0.0028$). However, bath application of Sp-cAMPs abolished all turning ($n = 10$, $p = 0.576$ from vehicle, $p = 0.08$ from STIM1-KD, Mann–Whitney *U* test). ***H***, Growth cone turning in response to sema-3a after STIM1-KD could be restored by activating cAMP signaling (all turning is compared with vehicle, random growth, $n = 23$). STIM1-CTRL growth cones turning away from a source of sema-3a ($n = 22$, $^{****}p = 0.000097$) was abolished after PKA activation with Sp-cAMPs ($n = 19$, $p = 0.09$ from vehicle, $^{**}p = 0.0077$ from STIM1-CTRL). STIM1-KD growth cones failed to turn away from a source of sema-3a ($n = 12$, $p = 0.56$). However, this turning was rescued with bath application of Sp-cAMPs ($n = 12$, $^{**}p = 0.0073$ from vehicle, $^{**}p = 0.0094$ from STIM1-KD, Mann–Whitney *U* test).

regardless of whether the guidance cue requires ER-calcium signals.

In addition to the regulation and localization of microtubules, there is a further mechanism that could explain the loss of growth cone steering in response to sema-3a after STIM1 knockdown. STIM1 is reported to interact with adenylate cyclase (Lefkimmiatis et al., 2009; Maiellaro et al., 2012), and it is well established that the ratio of cAMP to cGMP is crucial for growth cone steering (Ming et al., 1997; Song et al., 1997, 1998; Shelly et al., 2010; Nicol et al., 2011; Akiyama et al., 2016). Therefore, we asked whether we could restore growth cone steering away from sema-3a in STIM1-KD growth cones by pharmacologically altering cAMP signaling using Sp-cAMPs (20 μM) to activate protein kinase A (PKA). We found that activation of PKA restored repulsive turning to sema-3a but failed to rescue BDNF steering in STIM1-KD growth cones (Fig. 5*G*,*H*), suggesting that STIM1 regulation of growth cone turning is upstream of cyclic nucleotide signaling in response to sema-3a.

### STIM1 is required for axon guidance *in vivo*

Our *in vitro* data predict that reducing STIM1 expression *in vivo* alters calcium dynamics in pathfinding neurons, resulting in ab-

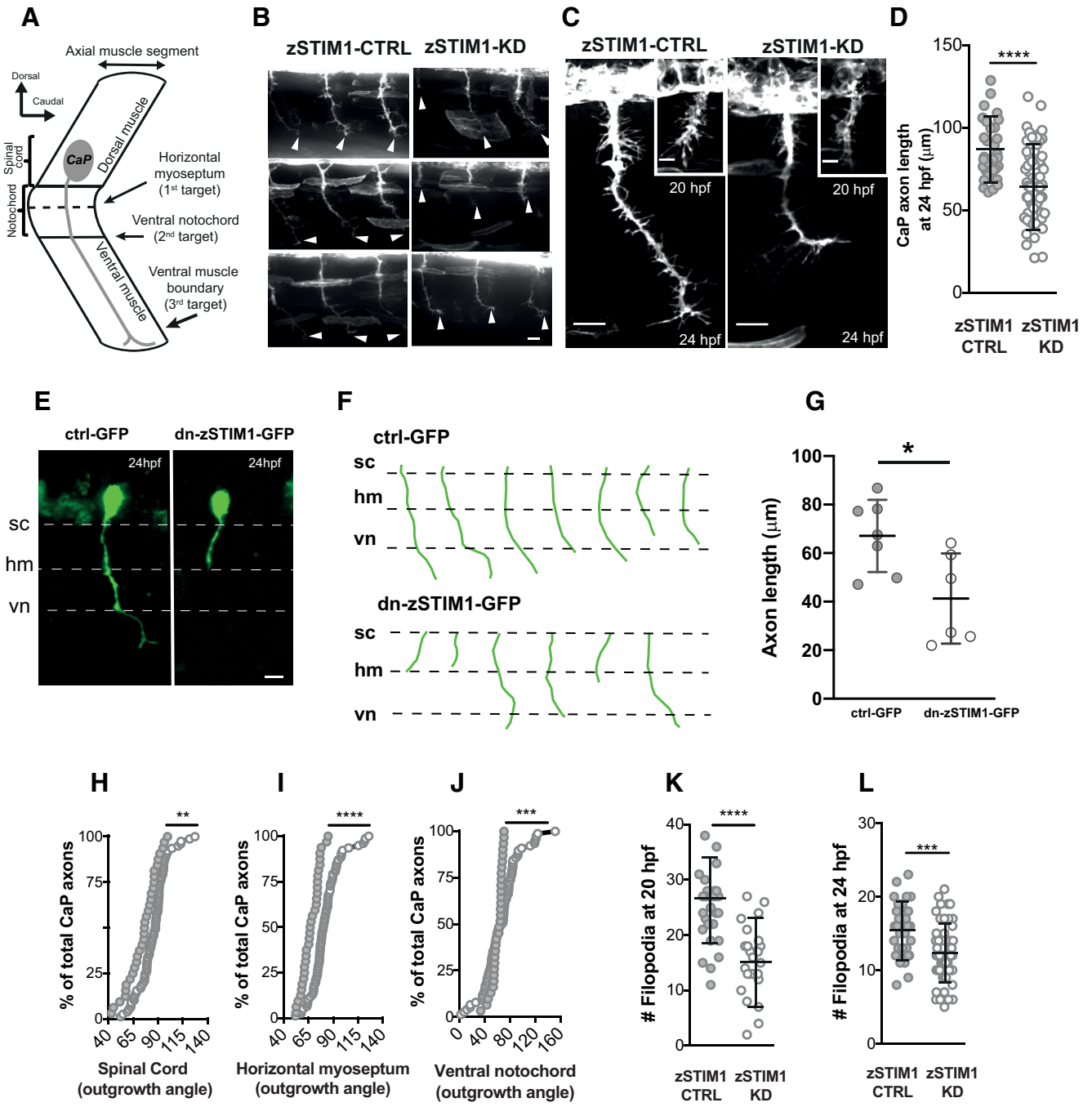


**Figure 6.** STIM1 is required for axon pathfinding by zebrafish CaP motor neurons *in vivo*. ***A***, Schematic illustrating the stereotypic axon pathfinding trajectory of CaP neurons from the zebrafish spinal cord. ***B***, ***C***, Representative images of CaP axons from zSTIM1 control (zSTIM1-CTRL) and zSTIM1-morphant (zSTIM1-KD) Gal4$^{s1020t}$/UAS:mCherry embryos. ***B***, Representative axon trajectories from somites 6–9 in zSTIM1-CTRL or zSTIM1-KD larvae at 24 hpf. Arrows indicate distal tips of CaP axons. Scale bar, 10 $\mu$m. ***C***, Individual zSTIM1-CTRL and zSTIM1-KD CaP axons at 20 hpf (inset) and 24 hpf. Scale bars: 20 hpf, 5 $\mu$m; 24 hpf, 10 $\mu$m. ***D***, Quantification of CaP axon length at 24 hpf in zSTIM1-CTRL ($n = 32$) and zSTIM1-KD ($n = 77$) embryos (****$p = 3.78E-06$, Mann–Whitney *U* test). ***E***, Representative examples of CaP neurons expressing control GFP or dn-zSTIM1-GFP at 24 hpf. Scale bar, 5 $\mu$m. ***F***, Tracings of axon trajectories of control GFP or dn-zSTIM1-GFP axons at 24 hpf. ***G***, Quantification of CaP axon length at 24 hpf in GFP-CTRL ($n = 7$) and dn-zSTIM1-GFP axons ($n = 6$, *$p = 0.022$, unpaired *t* test with Welch's correction). ***H–J***, Cumulative frequency distributions showing angles of outgrowth of zSTIM1-CTRL (closed circles) and zSTIM1 KD (open circles) CaP axons away from the (***H***) spinal cord (**$p = 0.0092$), (***I***) horizontal myoseptum (****$p = 7.06E-07$), and (***J***) ventral notochord (***$p = 0.0006$, Kolmogorov–Smirnov test). ***K***, ***L***, Number of filopodia on the distal 20 $\mu$m of CaP axons at (***K***) 20 hpf (****$p = 8.6E-07$) and (***L***) 24 hpf (***$p = 0.0007$, Mann–Whitney *U* test).

errant axon guidance. To examine this directly, we used morpholinos as well as a dominant-negative approach to perturb zSTIM1 function during development and analyzed motor axon pathfinding *in vivo*. The morpholinos included two independent translation-blocking zSTIM1 morpholinos, two control morpholinos: a 5′ mispaired and a p53 morpholino. We did not observe any significant differences between the two specific zSTIM1 morpholinos or between the control morpholinos, across mortality, developmental defects, or axon length (data not shown). Hence from herein, we refer to zSTIM1-control morphant and zSTIM1-specific morphant animals as zSTIM1-CTRL and zSTIM1-KD, respectively. We reduced zSTIM1 expression in

**Table 2. zSTIM1 is required for axon guidance *in vivo*[a]**

| | | zSTIM1-CTRL | zSTIM1-KD |
|---|---|---|---|
| Position of CaP axon distal tip at 24 hpf | Horizontal myoseptum | 0/32 | 4/78 |
| | Ventral notochord | 2/32 | 25/78 |
| | Ventral muscle boundary | 30/32 | 49/78 |
| Position of CaP axon distal tip at 48 hpf | Ventral notochord | 0/44 | 3/40 |
| | Ventral muscle boundary | 0/44 | 4/40 |
| | Entered lateral surface of muscle | 44/44 | 33/40 |

[a]zSTIM1-CTRL and zSTIM1-KD CaP axons were visualized in Gal4$^{s1020t}$/UAS:mCherry embryos, with axons scored on the position of the most distal aspect of the axon at 24 or 48 hpf. The number of axons located at each position is represented as a fraction of total number of CaP axons visualized (values represent the number of axons imaged in 27 zSTIM1-KD and 12 zSTIM1-CTRL embryos).

**Table 3. zSTIM1 is required for evoked motor function in zebrafish embryos and larvae[a]**

| | | zSTIM1-CTRL | zSTIM1-KD |
|---|---|---|---|
| Evoked coiling response at 28 hpf | Percentage of embryos displaying evoked coiling activity upon stimulation | 99.6 ± 0.4 | 59 ± 3.97 ($p = 0.0097$) |
| Startle response at 52 hpf | Mean distance moved (mm) | 5.826 ± 3.97 | 3.920 ± 2.97 ($p = 0.0044$) |

[a]The coiling response at 28 hpf is represented as the percentage of embryos that moved in response to tactile stimulation. zSTIM1-CTRL ($n = 242$) and zSTIM1-KD ($n = 183$) embryos were tested over 5 separate experiments from separate mating clutches. The startle response at 52 hpf was tested in zSTIM1-CTRL ($n = 55$) and zSTIM1-KD ($n = 63$) larvae over 3 separate experiments from separate mating clutches. Behavior was performed at 22°C. Statistical analysis was performed using the Mann–Whitney *U* test (28 hpf) and unpaired *t* test with Welch's correction (52 hpf).

Gal4$^{s1020t}$/UAS:mCherry zebrafish embryos (Scott et al., 2007; Heap et al., 2013), in which expression of mCherry in spinal motor neurons (Wyart et al., 2009) enabled visualization of extending axons and filopodia (Fig. 6). We selected CaP motor neurons for analysis because their axons exhibit highly stereotypic pathfinding trajectories as they exit the spinal cord and project toward the ventral muscle via the horizontal myoseptum and ventral notochord, in the absence of any other axons (Fig. 6*A*) (Myers et al., 1986; Eisen et al., 1989; Eisen, 1991; Plazas et al., 2013). Consistent with these previous reports, CaP axons navigated to ventral muscle by 24 hpf in zSTIM1-CTRL embryos (Fig. 6*B*,*C*; Table 2). However, in zSTIM1-KD embryos, we found an increase in the number CaP neurons that failed to extend to the ventral muscle by 24 hpf (Fig. 6*B*,*C*; Table 2). On closer examination, growth cones of zSTIM1-KD axons appeared to pause or stall at key intermediate targets, the horizontal myoseptum and ventral notochord (Fig. 6*C*; Table 2). Consistent with such a stalling phenotype, the length of CaP axons at 24 hpf was reduced in zSTIM1-KD embryos compared with zSTIM1-CTRL embryos (Fig. 6*D*). Interestingly, all control axons had navigated to the lateral surface of the ventral muscle by 48 hpf, whereas a number of zSTIM1-KD axons remained stalled at intermediate choice points (Table 2), suggesting a requirement for STIM1 expression for axon guidance *in vivo*.

To examine the cell-autonomous effect of perturbing zSTIM1 function on axon pathfinding, we overexpressed a GFP-tagged dominant negative form of zSTIM1 (dn-zSTIM1-GFP) in which zSTIM1 was truncated at residue 233 and the calcium binding residue within the EF-hand was mutated (D70A). The mutant protein perturbs endogenous STIM1 function, preforming puncta in absence of ER-calcium depletion, thereby failing to induce calcium influx via SOCE (Liou et al., 2005). To restrict dn-zSTIM1-GFP expression to motor neurons, we drove expression of dn-zSTIM1-GFP or GFP using the zebrafish motor neuron promotor, mnx1/Hb9 (Arkhipova et al., 2012). Consistent with zSTIM1 being necessary for axon pathfinding *in vivo*, axons expressing the dn-zSTIM1-GFP were observed to exhibit a stalling phenotype with reduced axon outgrowth, compared with GFP-expressing controls (Fig. 6*E*–*G*). The dn-zSTIM1-GFP phenotype was very similar to that displayed by the zSTIM1-KD axons (compare Fig. 6*E*–*G* with 6*B*–*D*).

Given that zSTIM1-KD CaP axons stalled at intermediate targets, we reasoned that these axons had failed to respond correctly to guidance signals at these key choice points. This supposition was supported by our observation that CaP axon length (Fig. 6*B*–*G*), and trajectories were altered at intermediate choice points, notably the spinal cord (Fig. 6*H*), horizontal myoseptum (Fig. 6*I*), and ventral notochord (Fig. 6*J*) in zSTIM1-KD embryos. Furthermore, filopodial protrusion was similarly perturbed when zSTIM1 expression was reduced. Significantly, zSTIM1-KD CaP axons elaborated significantly fewer filopodia at both 20 hpf (Fig. 6*K*) and 24 hpf (Fig. 6*L*). Consistent with our data demonstrating that STIM1 is necessary for growth cone steering in response to guidance cues *in vitro*, these results show that perturbation of zSTIM1 expression causes axons to exhibit aberrant guidance at intermediate choice points during pathfinding and suggest that zSTIM1 is necessary for axons to recognize and respond correctly to axon guidance signals *in vivo*. Because zSTIM1-KD axons and dn-zSTIM1-GFP axons displayed defects in axon pathfinding, we examined the effect of reducing STIM1 expression on motor function. As zSTIM1-KD and dn-zSTIM1-GFP axons displayed a stalled, or delayed phenotype at 24 hpf, with most axons ultimately reaching their targets by 48 hpf (Table 2), motor function was assessed using the evoked motor response at 28 and 52 hpf (Table 3). zSTIM1-KD animals displayed both coiling and startle reflex defects at both 28 and 52 hpf, suggesting that defects in muscle innervation persist, even though most axons reach the muscle at 48 hpf.

Given the key role of zSTIM1 in regulating calcium in navigating axons *in vitro*, we asked whether the perturbed axon guidance observed in zSTIM1-KD animals is due to aberrant calcium signaling in motor axons as they navigate *in vivo*. We first confirmed that zebrafish spinal motor neurons exhibit zSTIM1-mediated SOCE, by performing calcium imaging in cultured spinal motor neurons (Andersen, 2001; Chen et al., 2013). Cells were treated with thapsigargin (5 $\mu$M), in the absence of extracellular calcium, to deplete ER-calcium stores. The restoration of calcium (2.5 mM) to the extracellular medium triggered SOCE, as shown by a significant increase in intracellular calcium in zSTIM1-CTRL spinal motor neurons (Fig. 7*A*,*B*). In contrast, neurons from zSTIM1-KD embryos showed a significantly reduced calcium influx when SOCE was evoked (Fig. 7*A*,*B*), confirming that zSTIM1 activates SOCE in zebrafish spinal motor neurons and also confirming that the zSTIM1a morpholino effectively reduced zSTIM1 function in zebrafish.

Calcium signaling is key to axon guidance at choice points *in vivo* (Gomez and Spitzer, 1999; Plazas et al., 2013), so we next examined the role of zSTIM1 in regulating calcium signaling in CaP neurons as axons navigate intermediate choice points. We imaged calcium dynamics in CaP axons of zSTIM1-CTRL or zSTIM1-KD Gal4$^{s1020t}$/UAS:GCaMP5 embryos as axons navigated the horizontal myoseptum (Fig. 7*C*–*H*). In zSTIM1-CTRL embryos, the patterns of calcium activity were consistent with previous studies, showing an increase in activity as axons navigated the myoseptum and postmyoseptum (Fig. 7*C*,*D*) (Plazas et al., 2013). Many CaP axons of zSTIM1-KD embryos exhibited no spiking during the imaging period (data not shown); and in cells that did show activity, the frequency of calcium signals was significantly reduced compared with control CaP axons at the my-

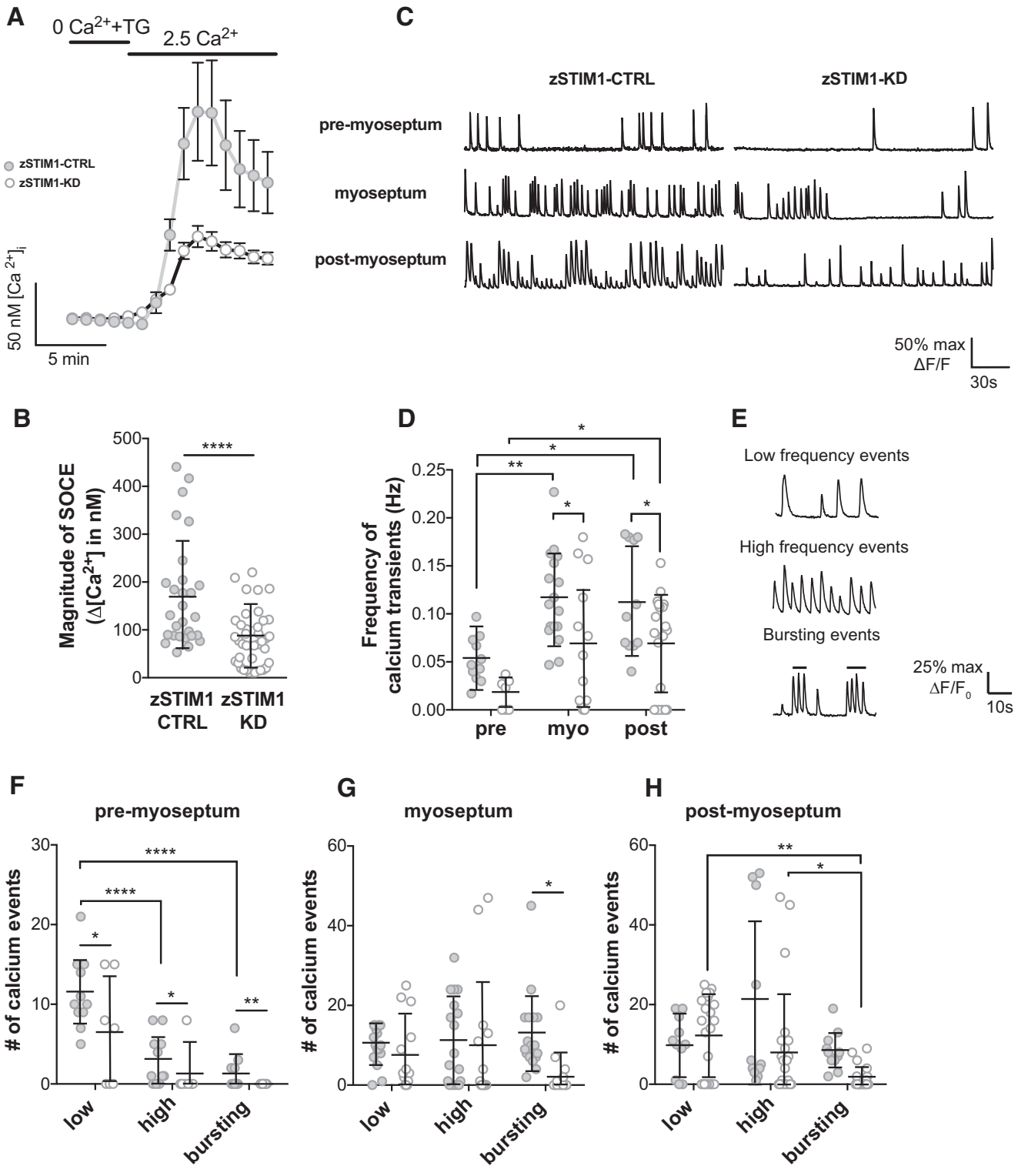


**Figure 7.** STIM1 is required for patterning of calcium events in navigating axons *in vivo*. ***A***, ***B***, fura-2 $Ca^{2+}$ imaging was used to measure SOCE in spinal motor neurons isolated from zSTIM1 control (zSTIM1-CTRL) and zSTIM1-morphant (zSTIM1-KD) embryos. SOCE was triggered *in vitro* by incubating neurons in 0 mM $Ca^{2+}$ media with 5 $\mu$M thapsigargin followed by the addition of 2.5 mM $Ca^{2+}$ media. ***A***, Average fura-2 $Ca^{2+}$ traces of zSTIM1-CTRL ($n = 28$) and zSTIM1-KD ($n = 42$) spinal motor neurons. ***B***, Quantification of SOCE magnitude, calculated as the change in [$Ca^{2+}$]i upon the addition of 2.5 mM $Ca^{2+}$ media, in zSTIM1-CTRL and zSTIM1-KD spinal motor neurons (****$p = 0.00003$, Student's *t* test). ***C–H***, Axonal calcium events were measured in CaP axons of zSTIM1-CTRL and zSTIM1-KD Gal4s1020t/UAS:GCaMP5G embryos. ***C***, Representative calcium responses from CaP axons of zSTIM1-CTRL or zSTIM1-KD located proximal to the horizontal myoseptum (premyoseptum), at the horizontal myoseptum, or distal to the horizontal myoseptum (postmyoseptum). ***D***, Frequency of calcium events quantified at each stage of axon outgrowth in zSTIM1-CTRL ($n =$ 11 axons from 7 embryos) and zSTIM1-KD embryos ($n = 17$ axons from 13 embryos). zSTIM1-CTRL axons displayed an increase in frequency of calcium transients at the myoseptum (**$p = 0.0035$) and postmyoseptum (*$p = 0.0104$) compared with the premyoseptum. In contrast in zSTIM1-KD axons, the change in frequency of calcium transients only increased at the postmyoseptum compared with the premyoseptum (*$p = 0.0403$). Significantly, reduced STIM1 expression attenuated the frequency of calcium events at the myoseptum (*$p = 0.0298$) and postmyoseptum (*$p =$ 0. 0.0453), compared with zSTIM1-CTRL (two-way ANOVA with Holm–Sidak test for multiple comparisons). ***E***, Representative traces illustrate low-frequency ($<$7.5 spikes·min $^{-1}$), high-frequency ($\geq$7.5 spikes·min $^{-1}$), and bursting ($\geq$15 spikes·min $^{-1}$) calcium events observed in CaP axons. ***F–H***, Calcium events were quantified in CaP axons of zSTIM1-CTRL (*Figure legend continues.*)

oseptum and postmyoseptum (Fig. 7*C*,*D*). Calcium spiking activity was classified as low-frequency, high-frequency, or bursting events (Fig. 7*E*) as described previously (Plazas et al., 2013). Low-frequency events were the predominant pattern of calcium activity in axons premyoseptum, and these were significantly attenuated in zSTIM1-KD axons (Fig. 7*F*). Conversely, high-frequency and bursting signals predominated in axons located at the myoseptum (Fig. 7*G*) and postmyoseptum (Fig. 7*H*), consistent with navigation behavior described previously (Gomez and Spitzer, 1999; Plazas et al., 2013). Significantly, zSTIM1 axons displayed significantly fewer bursting calcium signals at the myoseptum and post-myoseptum (Fig. 7*G*,*H*). These data indicate that attenuated bursting activity in zSTIM1-KD embryos correlates with excessive pausing or stalled axon guidance at choice points and suggests that zSTIM1-mediated calcium signaling is required to transduce environmental guidance cues into pathfinding decisions *in vivo*.

## Discussion

Growth cone navigation relies on guidance cue activation of signaling cascades that bias the localization of steering machinery, such as microtubules and ER, to one side of the growth cone, thereby converting random growth to attractive, or repulsive turning. STIM1, a key regulator of SOCE, is required for growth cone navigation in response to ER-calcium-dependent guidance cues, such as BDNF and the ER-calcium-independent cue, sema-3a (Mitchell et al., 2012). However, the mechanism by which STIM1 regulates growth cone steering in response to such heterogeneous guidance cues is unknown. Here, we reveal that, in addition to SOCE, STIM1 plays a second, equally important function in growth cones: regulating microtubule and ER remodeling to motile regions of navigating growth cones.

### STIM1-EB interactions regulate ER-microtubule association in steering growth cones

In eukaryotic cells, the close association of ER and microtubules is regulated by polymerization-mediated tip attachment complexes (Waterman-Storer and Salmon, 1998; Akhmanova and Steinmetz, 2008) and microtubule-associated molecular motors (Allan and Vale, 1991). However, the mechanisms that control ER localization in highly motile structures, such as growth cones, remain unclear. Electron microscopy studies have demonstrated cross-bridging between microtubules and ER along microtubule shafts in growth cones (Dailey and Bridgman, 1991), which could represent STIM1-EB interactions. Several studies have examined the role of STIM1-mediated SOCE in cell migration, but few have examined the effect of STIM1-EB interactions on ER motility. For example, in a recent study, Chang et al. (2018) demonstrated that STIM1-EB interactions sequestered STIM1 at microtubules, preventing STIM1 from prematurely moving to junctions of ER-plasma membrane and activating excessive calcium influx. However, they did not examine the effect of the STIM1-EB interaction on ER remodeling or cell motility (Chang et al., 2018). In smooth muscle and cancer cells, STIM1 expression and phosphorylation are necessary for cell migration and formation of focal adhesions (Bisaillon et al., 2010; Chen et al., 2011; Casas-Rua et al., 2015). STIM1-EB interactions are important for localizing calcium signals toward the leading edge of migrating cells, although the role of STIM1 in regulating ER remodeling was not examined (Tsai et al., 2014). Here, we provide the first evidence that STIM1 is required for microtubule and ER remodeling into filopodia and suggest a mechanism whereby STIM1-EB interactions tether ER to microtubules to regulate the spatiotemporal localization of calcium release machinery to motile areas of steering growth cones.

The guidance of primary motor axons in zebrafish is directed by a number of guidance cues, including semaphorins and myotome-derived cues (Beattie et al., 2000; Halloran et al., 2000; Zeller et al., 2002; Schneider and Granato, 2006; Plazas et al., 2013), with stalling at intermediate targets a common outcome after guidance cue disruption. We found that reducing zSTIM1 expression *in vivo* perturbed calcium signaling in motor axons at intermediate axon guidance choice points, with axons displaying decreased filopodial number, axon stalling, and delayed extension. zSTIM1 was required for SOCE in these axons, demonstrating that zSTIM1a plays an important role in calcium regulation in zebrafish motor neurons, although we cannot rule out a function for zSTIM1b. The changes we observed in calcium signaling at multiple choice points *in vivo*, combined with our *in vitro* data demonstrating that growth cones require STIM1 function to respond to multiple guidance cues, supports the hypothesis that STIM1 is necessary for axon guidance *in vivo*.

Growth cone filopodia are considered the "first responders" of axon guidance (Tosney and Landmesser, 1985; Chien et al., 1993; Davenport et al., 1993; Polinsky et al., 2000), transmitting molecular guidance signals to the growth cone central domain through receptor-mediated calcium transients (Gomez and Letourneau, 1994; Goodhill and Urbach, 1999; Gomez et al., 2001). STIM1-mediated control of microtubules and ER remodeling could subserve at least four crucial functions in growth cone filopodia. First, the STIM1-EB interactions at microtubule plus-ends enhanced ER recruitment into filopodia. Early studies predicted that filopodia containing ER, or with ER at the filopodial base, might respond differently to external guidance cues than those filopodia without associated ER (Davenport et al., 1996). Consistent with this, reducing STIM1 expression perturbed axon guidance *in vitro* and *in vivo*. Second, calcium transients initiated at distal filopodia are amplified and sustained by calcium release from the ER and subsequent SOCE (Gomez and Letourneau, 1994; Davenport et al., 1996; Shim et al., 2013). These calcium signals could propagate proximally to areas of microtubule reorganization in central areas of the growth cone, precipitating remodeling of microtubules and ER toward the motile side of growth cones. Third, STIM1-mediated SOCE in filopodia would favor the formation of ER-plasma membrane junctions, thought to be important for growth cone consolidation and extension (Davenport et al., 1996). Last, tubular ER is recognized as a wholly interconnected and continuous membrane in eukaryotes (Terasaki et al., 1994; Petersen et al., 2001; Wu et al., 2017). Such a calcium-rich network of organelles would facilitate the conduction of calcium signals from filopodia throughout the growth cone via ER micro-networks (Choi et al., 2006). For example, ER-calcium depletion in peripheral areas of growth cones can be signaled to the growth cone central domain directing further ER remodeling and subsequent localization of instructive calcium signals necessary for steering.

←

(*Figure legend continued.*) and zSTIM1-KD. ***F***, At the premyoseptum, low-frequency calcium activity predominated and was significantly reduced in zSTIM1-KD compared with zSTIM1-CTRL (*$p = 0.0238$). ***G***, At the myoseptum, bursting calcium activity was significantly reduced in zSTIM1-KD compared with zSTIM1-CTRL (*$p = 0.0212$). ***H***, At the postmyoseptum, bursting calcium activity was significantly reduced in zSTIM1-KD compared with zSTIM1-CTRL (*$p = 0.0477$, two-way ANOVA with Holm–Sidak test for multiple comparisons). ***A***, The key applies to graphs in ***B***, ***C***, ***F–H***: closed circles represent zSTIM1-CTRL; open circles represent zSTIM1-KD.

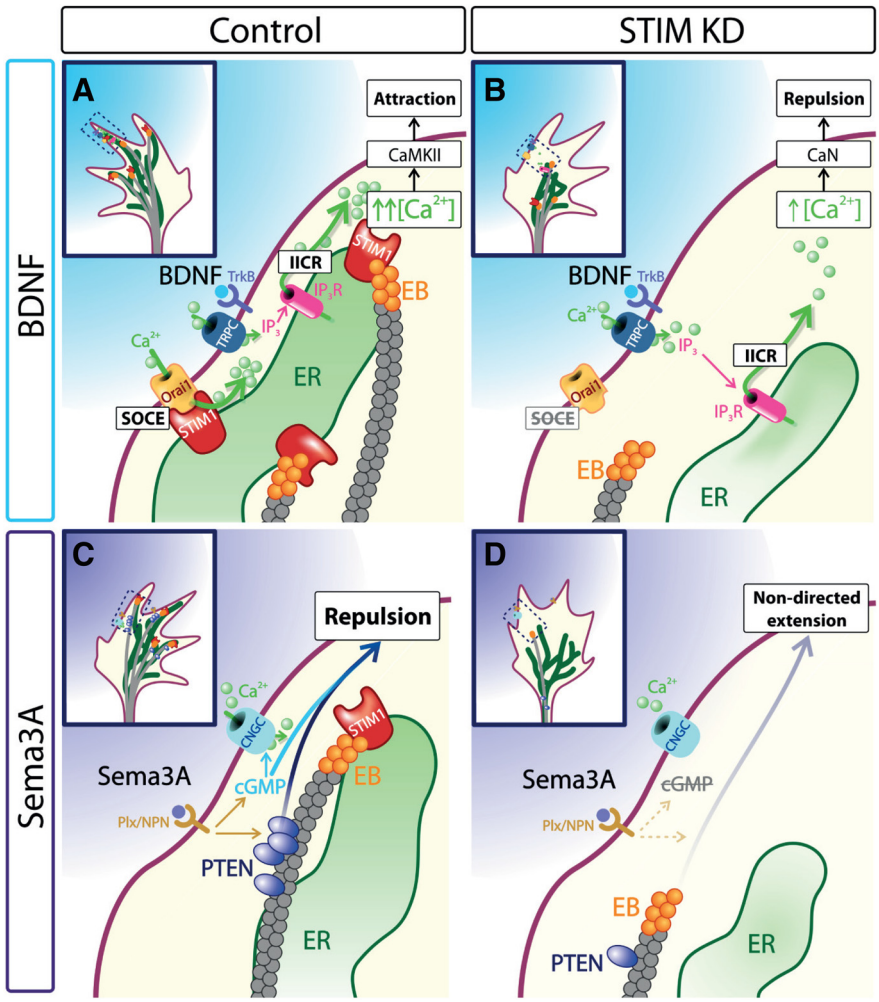


**Figure 8.** STIM1 mediates ER-microtubule remodeling into filopodia to localize $Ca^{2+}$ signals in motile growth cones. Schematic illustrating a model for STIM1-dependent ER remodeling into growth cone filopodia via direct interaction between STIM1 and EB proteins at microtubule plus-ends. STIM1 is a multifunctional protein in growth cones that acts as a microtubule-plus-end tracking protein and an activator of SOCE to regulate (1) ER remodeling with polymerizing microtubules into the growth cone periphery to localize ER-derived $Ca^{2+}$ signals, and (2) facilitate refilling of the ER $Ca^{2+}$ store via SOCE to sustain compartmentalized $Ca^{2+}$ signaling in filopodia. ***A***, This model illustrates how STIM1 functions downstream of ER calcium-dependent guidance cue BDNF to mediate growth cone turning towards the guidance cue (inset in A). ***B***, When STIM1 expression is reduced, the interaction between the ER and microtubules is lost and there is a reduced calcium signal, resulting in the growth cone turning away from the source of BDNF (inset B). ***C***, This model illustrates how STIM1 functions downstream of ER calcium-independent guidance cue sema-3a to mediate growth cone turning away from the guidance cue (inset C). ***D***, When STIM1 expression is reduced, the loss of the microtubule organization reduces the supply of PTEN to the membrane and results in the growth cones no longer turning in response to sema-3a, instead growing in a random direction (inset D).

### STIM1 functions downstream of multiple guidance cues during growth cone navigation

This study reveals dual functions for STIM1 in growth cone steering in response to attractive and repulsive guidance cues (Fig. 8). Our data support the well-described model of attractive guidance cues, such as BDNF or netrin-1 activating calcium influx through TRPC channels (Li et al., 2005; Wang and Poo, 2005; Gasperini et al., 2009), triggering calcium release via inositol triphosphate or ryanodine receptor activation on the ER membrane (for review, see Tojima et al., 2011). This release of store calcium activates STIM1 and subsequent refilling of the ER via SOCE, which sustains guidance cue-induced elevations in intracellular calcium (Mitchell et al., 2012). Sustained asymmetric calcium signals activate downstream CaMKII (Wen et al., 2004) and calcium-dependent activation of membrane exocytosis via VAMP2 (Tojima et al., 2007), biasing growth cone motility toward the source of guidance cue. Conversely, reduced STIM1 expression significantly attenuates calcium signal amplitude, causing a switch from attraction to repulsion (Mitchell et al., 2012), consistent with calcineurin activation (Wen et al., 2004). Here, we propose that the interaction of STIM1 with microtubules is critical to generate localized ER-mediated calcium signals, biasing the steering machinery toward the motile side of the growth cone (Fig. 8*A*,*B*).

Growth cone repulsion operates through distinctly different mechanisms to growth cone attraction (Tojima et al., 2007; Henle et al., 2013; Akiyama et al., 2016). sema-3a-induced repulsion requires cyclic nucleotide-dependent exocytosis, mediated by VAMP7 (Akiyama et al., 2016), actin recruitment via mical (Hung et al., 2010), and phosphatase and tensin homolog, PTEN, activity (Henle et al., 2013). How, then, does decreased STIM1 expression perturb sema-3a-induced repulsion? There are at least two points of intersection between sema-3a and STIM1 signaling: cyclic nucleotides and PTEN. First, STIM1 activates SOCE-dependent cAMP signaling (Lefkimmiatis et al., 2009). Given that sema-3a function requires cGMP signaling (Song et al., 1998) and there is reciprocal cross talk between cAMP and cGMP (Shelly et al., 2010), a reduction of STIM1 expression could disrupt the cAMP/cGMP ratio and hence perturb growth cone repulsion. Consistent with this, we could restore sema-3a-induced repulsion in growth cones with reduced STIM1 expression by pharmacological manipulation of cAMP signaling, suggesting that cyclic nucleotide signaling is downstream of sema-3a-mediated STIM1 signaling (Fig. 8*C*,*D*). Second, sema-3a requires PTEN activation to trigger growth cone repulsion (Henle et al., 2013). PTEN closely associates with microtubules and remodels growth cone focal adhesions (Chadborn et al., 2006; Henle et al., 2013). PTEN is thought to be sequestered to microtubules; and upon sema-3a activation, PTEN is released from dynamic microtubules in the growth cone periphery and targeted to the plasma membrane. At the membrane, PTEN inhibits activation of signaling lipid phosphatidylinositol (3,4,5)-triphosphate while also decreasing the phosphorylation status of GSK-3$\beta$, thereby decreasing assembly of the microtubule and actin cytoskeleton (Zhou et al., 2004; Chadborn et al., 2006; Henle et al., 2013). We therefore propose that microtubules are the key point of convergence between sema-3a and STIM1 signaling pathways, with STIM1-EB-mediated remodeling of microtubules representing a vital supply of PTEN to the membrane, necessary for growth cone repulsion (Fig. 8*C*,*D*).

In conclusion, we demonstrate that STIM1 is required for dynamic EB localization and the remodeling of microtubules and ER in navigating growth cones. The observation that drebrin is

upregulated in growth cones and filopodia when STIM1 is reduced, illustrates a complex interplay of compensatory signals acting between the microtubule and actin cytoskeleton to control growth cone motility. The fact that upregulation of drebrin at the growth cone periphery was not sufficient to restore directed microtubule protrusion in STIM1-KD growth cones strongly suggests that STIM1 is a principal regulator of instructional signals in filopodia during motility and subsequent ER remodeling. In conclusion, these data demonstrate that, in addition to the activation of SOCE, STIM1 regulates microtubule and ER remodeling, which is a common mechanism activated by multiple guidance cues and is vital in growth cone steering and axon guidance *in vivo*.

## References


Akhmanova A, Steinmetz MO (2008) Tracking the ends: a dynamic protein network controls the fate of microtubule tips. Nat Rev Mol Cell Biol 9:309–322.

Akiyama H, Fukuda T, Tojima T, Nikolaev VO, Kamiguchi H (2016) Cyclic nucleotide control of microtubule dynamics for axon guidance. J Neurosci 36:5636–5649.

Allan VJ, Vale RD (1991) Cell cycle control of microtubule-based membrane transport and tubule formation in vitro. J Cell Biol 113:347–359.

Andersen SS (2001) Preparation of dissociated zebrafish spinal neuron cultures. Methods Cell Sci 23:205–209.

Arkhipova V, Wendik B, Devos N, Ek O, Peers B, Meyer D (2012) Characterization and regulation of the hb9/mnx1 beta-cell progenitor specific enhancer in zebrafish. Dev Biol 365:290–302.

Asanov A, Sherry R, Sampieri A, Vaca L (2013) A relay mechanism between EB1 and APC facilitates STIM1 puncta assembly at endoplasmic reticulum-plasma membrane junctions. Cell Calcium 54:246–256.

Beattie CE, Melancon E, Eisen JS (2000) Mutations in the stumpy gene reveal intermediate targets for zebrafish motor axons. Development 127: 2653–2662.

Beetz C, Johnson A, Schuh AL, Thakur S, Varga RE, Fothergill T, Hertel N, Bomba-Warczak E, Thiele H, Nürnberg G, Altmüller J, Saxena R, Chapman ER, Dent EW, Nürnberg P, Audhya A (2013) Inhibition of TFG function causes hereditary axon degeneration by impairing endoplasmic reticulum structure. Proc Natl Acad Sci U S A 110:5091–5096.

Bill BR, Petzold AM, Clark KJ, Schimmenti LA, Ekker SC (2009) A primer for morpholino use in zebrafish. Zebrafish 6:69–77.

Bisaillon JM, Motiani RK, Gonzalez-Cobos JC, Potier M, Halligan KE, Alzawahra WF, Barroso M, Singer HA, Jourd'heuil D, Trebak M (2010) Essential role for STIM1/Orai1-mediated calcium influx in PDGF-induced smooth muscle migration. Am J Physiol Cell Physiol 298:C993–C1005.

Blackstone C (2012) Cellular pathways of hereditary spastic paraplegia. Annu Rev Neurosci 35:25–47.

Buck KB, Zheng JQ (2002) Growth cone turning induced by direct local modification of microtubule dynamics. J Neurosci 22:9358–9367.

Casas-Rua V, Tomas-Martin P, Lopez-Guerrero AM, Alvarez IS, Pozo-Guisado E, Martin-Romero FJ (2015) STIM1 phosphorylation triggered by epidermal growth factor mediates cell migration. Biochim Biophys Acta 1853:233–243.

Chadborn NH, Ahmed AI, Holt MR, Prinjha R, Dunn GA, Jones GE, Eickholt BJ (2006) PTEN couples Sema3A signalling to growth cone collapse. J Cell Sci 119:951–957.

Chang CL, Chen YJ, Quintanilla CG, Hsieh TS, Liou J (2018) EB1 binding restricts STIM1 translocation to ER-PM junctions and regulates store-operated $Ca^{2+}$ entry. J Cell Biol 217:2047–2058.

Chen L, Meng Q, Jing X, Xu P, Luo D (2011) A role for protein kinase C in the regulation of membrane fluidity and $Ca^{2}(+)$ flux at the endoplasmic reticulum and plasma membranes of HEK293 and Jurkat cells. Cell Signal 23:497–505.

Chen Z, Lee H, Henle SJ, Cheever TR, Ekker SC, Henley JR (2013) Primary neuron culture for nerve growth and axon guidance studies in zebrafish (*Danio rerio*). PLoS One 8:e57539-e57611.

Chien CB, Rosenthal DE, Harris WA, Holt CE (1993) Navigational errors made by growth cones without filopodia in the embryonic *Xenopus* brain. Neuron 11:237–251.

Choi YM, Kim SH, Chung S, Uhm DY, Park MK (2006) Regional interaction of endoplasmic reticulum $Ca^{2+}$ signals between soma and dendrites through rapid luminal $Ca^{2+}$ diffusion. J Neurosci 26:12127–12136.

Cohan CS, Connor JA, Kater SB (1987) Electrically and chemically mediated increases in intracellular calcium in neuronal growth cones. J Neurosci 7:3588–3599.

Dailey ME, Bridgman PC (1991) Structure and organization of membrane organelles along distal microtubule segments in growth cones. J Neurosci Res 30:242–258.

Davenport RW, Dou P, Rehder V, Kater SB (1993) A sensory role for neuronal growth cone filopodia. Nature 361:721–724.

Davenport RW, Dou P, Mills LR, Kater SB (1996) Distinct calcium signaling within neuronal growth cones and filopodia. J Neurobiol 31:1–15.

de Juan-Sanz J, Holt GT, Schreiter ER, de Juan F, Kim DS, Ryan TA (2017) Axonal endoplasmic reticulum $Ca^{2+}$ content controls release probability in CNS nerve terminals. Neuron 93:867–881.e6.

Dent EW, Callaway JL, Szebenyi G, Baas PW, Kalil K (1999) Reorganization and movement of microtubules in axonal growth cones and developing interstitial branches. J Neurosci 19:8894–8908.

Don EK, Formella I, Badrock AP, Hall TE, Morsch M, Hortle E, Hogan A, Chow S, Gwee SS, Stoddart JJ, Nicholson G, Chung R, Cole NJ (2017) A Tol2 gateway-compatible toolbox for the study of the nervous system and neurodegenerative disease. Zebrafish 144:69–72.

Eisen JS (1991) Developmental neurobiology of the zebrafish. J Neurosci 11:311–317.

Eisen JS, Pike SH, Debu B (1989) The growth cones of identified motoneurons in embryonic zebrafish select appropriate pathways in the absence of specific cellular interactions. Neuron 2:1097–1104.

Feske S, Gwack Y, Prakriya M, Srikanth S, Puppel SH, Tanasa B, Hogan PG, Lewis RS, Daly M, Rao A (2006) A mutation in Orai1 causes immune deficiency by abrogating CRAC channel function. Nature 441:179–185.

Gallo G, Letourneau PC (1998) Localized sources of neurotrophins initiate axon collateral sprouting. J Neurosci 18:5403–5414.

Gallo G, Letourneau PC (1999) Different contributions of microtubule dynamics and transport to the growth of axons and collateral sprouts. J Neurosci 19:3860–3873.

Gasperini R, Choi-Lundberg D, Thompson MJ, Mitchell CB, Foa L (2009) Homer regulates calcium signalling in growth cone turning. Neural Dev 4:29.

Geraldo S, Khanzada UK, Parsons M, Chilton JK, Gordon-Weeks PR (2008) Targeting of the F-actin-binding protein drebrin by the microtubule plus-tip protein EB3 is required for neuritogenesis. Nat Cell Biol 10:1181–1189.

Gomez TM, Letourneau PC (1994) Filopodia initiate choices made by sensory neuron growth cones at laminin/fibronectin borders in vitro. J Neurosci 14:5959–5972.

Gomez TM, Spitzer NC (1999) In vivo regulation of axon extension and pathfinding by growth-cone calcium transients. Nature 397:350–355.

Gomez TM, Spitzer NC (2000) Regulation of growth cone behavior by calcium: new dynamics to earlier perspectives. J Neurobiol 44:174–183.

Gomez TM, Robles E, Poo M, Spitzer NC (2001) Filopodial calcium transients promote substrate-dependent growth cone turning. Science 291: 1983–1987.

Goodhill GJ, Urbach JS (1999) Theoretical analysis of gradient detection by growth cones. J Neurobiol 41:230–241.

Grigoriev I, Gouveia SM, van der Vaart B, Demmers J, Smyth JT, Honnappa S, Splinter D, Steinmetz MO, Putney JW Jr, Hoogenraad CC, Akhmanova A (2008) STIM1 is a MT-plus-end-tracking protein involved in remodeling of the ER. Curr Biol 18:177–182.

Gu X, Spitzer NC (1995) Distinct aspects of neuronal differentiation encoded by frequency of spontaneous $Ca^{2+}$ transients. Nature 375:784–787.

Halloran MC, Sato-Maeda M, Warren JT Jr, Su F, Lele Z, Krone PH, Kuwada JY, Shoji W (2000) Laser-induced gene expression in specific cells of transgenic zebrafish. Development 127:1953–1960.

Heap LA, Goh CC, Kassahn KS, Scott EK (2013) Cerebellar output in zebrafish: an analysis of spatial patterns and topography in eurydendroid cell projections. Front Neural Circuits 7:53.

Henle SJ, Carlstrom LP, Cheever TR, Henley JR (2013) Differential role of PTEN phosphatase in chemotactic growth cone guidance. J Biol Chem 288:20837–20842.

Hong K, Nishiyama M, Henley J, Tessier-Lavigne M, Poo M (2000) Calcium signalling in the guidance of nerve growth by netrin-1. Nature 403:93–98.

Honnappa S, Gouveia SM, Weisbrich A, Damberger FF, Bhavesh NS, Jawhari H, Grigoriev I, van Rijssel FJ, Buey RM, Lawera A, Jelesarov I, Winkler FK, Wüthrich K, Akhmanova A, Steinmetz MO (2009) An EB1-binding motif acts as a microtubule tip localization signal. Cell 138:366–376.

Huang, GN, Zeng, W, Kim, JY, Yuan, JP, Han, L, Muallem, S, Worley, PF (2006) STIM1 carboxyl-terminus activates native SOC, *Icrac* and TRPC1 channels. Nat Cell Biol. 8:1003–1010.

Hung RJ, Yazdani U, Yoon J, Wu H, Yang T, Gupta N, Huang Z, van Berkel WJ, Terman JR (2010) Mical links semaphorins to F-actin disassembly. Nature 463:823–827.

Kwan KM, Fujimoto E, Grabher C, Mangum BD, Hardy ME, Campbell DS, Parant JM, Yost HJ, Kanki JP, Chien CB (2007) The Tol2kit: a multisite gateway-based construction kit for Tol2 transposon trans-genesis constructs. Dev Dyn 236:3088–3099.

Kyung T, Lee S, Kim JE, Cho T, Park H, Jeong YM, Kim D, Shin A, Kim S, Baek J, Kim J, Kim NY, Woo D, Chae S, Kim CH, Shin HS, Han YM, Kim D, Heo WD (2015) Optogenetic control of endogenous $Ca^{2+}$ channels in vivo. Nat Biotechnol 33:1092–1096.

Lefkimmiatis K, Srikanthan M, Maiellaro I, Moyer MP, Curci S, Hofer AM (2009) Store-operated cyclic AMP signalling mediated by STIM1. Nature 11:433–442.

Li HS, Xu XZ, Montell C (1999) Activation of a TRPC3-dependent cation current through the neurotrophin BDNF. Neuron 24:261–273.

Li Y, Jia YC, Cui K, Li N, Zheng ZY, Wang YZ, Yuan XB (2005) Essential role of TRPC channels in the guidance of nerve growth cones by brain-derived neurotrophic factor. Nature 434:894–898.

Liou, J, Kim, ML, Heo, WD, Jones, JT, Myers, JW, Ferrell Jr, JE, Meyer, T (2005) STIM is a $Ca^{2+}$ sensor essential for $Ca^{2+}$-store-depletion-triggered $Ca^{2+}$ influx. Curr Biol. 15:1235–1241.

Luik RM, Wu MM, Buchanan J, Lewis RS (2006) The elementary unit of store-operated $Ca^{2+}$ entry: local activation of CRAC channels by STIM1 at ER-plasma membrane junctions. J Cell Biol 174:815–825.

Maiellaro I, Lefkimmiatis K, Moyer MP, Curci S, Hofer AM (2012) Termination and activation of store-operated cyclic AMP production. J Cell Mol Med 16:2715–2725.

Merriam, EB, Millette, M, Lumbard, DC, Saengsawang, W, Fothergill, T, Hu, X, Ferhat, L, Dent, EW (2013) Synaptic regulation of microtubule dynamics in dendritic spines by calcium, F-actin, and drebrin. J Neurosci 33: 16471–16482.

Ming GL, Song HJ, Berninger B, Holt CE, Tessier-Lavigne M, Poo MM (1997) cAMP-dependent growth cone guidance by netrin-1. Neuron 19: 1225–1235.

Ming G, Song H, Berninger B, Inagaki N, Tessier-Lavigne M, Poo M (1999) Phospholipase C-gamma and phosphoinositide 3-kinase mediate cytoplasmic signaling in nerve growth cone guidance. Neuron 23:139–148.

Mitchell CB, Gasperini RJ, Small DH, Foa L (2012) STIM1 is necessary for store-operated calcium entry in turning growth cones. J Neurochem 122: 1155–1166.

Myers PZ, Eisen JS, Westerfield M (1986) Development and axonal outgrowth of identified motoneurons in the zebrafish. J Neurosci 6:2278–2289.

Nicol X, Hong KP, Spitzer NC (2011) Spatial and temporal second messenger codes for growth cone turning. Proc Natl Acad Sci U S A 108: 13776–13781.

Nishiyama M, von Schimmelmann MJ, Togashi K, Findley WM, Hong K (2008) Membrane potential shifts caused by diffusible guidance signals direct growth-cone turning. Nat Neurosci 11:762–771.

Nozawa K, Lin Y, Kubodera R, Shimizu Y, Tanaka H, Ohshima T (2017) Zebrafish Mecp2 is required for proper axonal elongation of motor neurons and synapse formation. Dev Neurobiol 77:1101–1113.

Ooashi N, Futatsugi A, Yoshihara F, Mikoshiba K, Kamiguchi H (2005) Cell adhesion molecules regulate $Ca^{2+}$-mediated steering of growth cones via cyclic AMP and ryanodine receptor type 3. J Cell Biol 170:1159–1167.

Petersen OH, Tepikin A, Park MK (2001) The endoplasmic reticulum: one continuous or several separate Ca(2+) stores? Trends Neurosci 24:271–276.

Pham E, Mills E, Truong K (2011) A synthetic photoactivated protein to generate local or global $Ca^{2+}$ signals. Chem Biol 18:880–890.

Plazas PV, Nicol X, Spitzer NC (2013) Activity-dependent competition regulates motor neuron axon pathfinding via PlexinA3. Proc Natl Acad Sci U S A 110:1524–1529.

Polinsky M, Balazovich K, Tosney KW (2000) Identification of an invariant response: stable contact with Schwann cells induces veil extension in sensory growth cones. J Neurosci 20:1044–1055.

Roos J, DiGregorio PJ, Yeromin AV, Ohlsen K, Lioudyno M, Zhang S, Safrina O, Kozak JA, Wagner SL, Cahalan MD, Veliçelebi G, Stauderman KA (2005) STIM1, an essential and conserved component of store-operated $Ca^{2+}$ channel function. J Cell Biol 169:435–445.

Saint-Amant L, Drapeau P (1998) Time course of the development of motor behaviors in the zebrafish embryo. J Neurobiol 37:622–632.

Schmunk G, Boubion BJ, Smith IF, Parker I, Gargus JJ (2015) Shared functional defect in IP3R-mediated calcium signaling in diverse monogenic autism syndromes. Transl Psychiatry 5:e643.

Schmunk G, Nguyen RL, Ferguson DL, Kumar K, Parker I, Gargus JJ (2017) High-throughput screen detects calcium signaling dysfunction in typical sporadic autism spectrum disorder. Sci Rep 7:40740–40749.

Schneider VA, Granato M (2006) The myotomal diwanka (lh3) glycosyltransferase and type XVIII collagen are critical for motor growth cone migration. Neuron 50:683–695.

Scott EK, Baier H (2009) The cellular architecture of the larval zebrafish tectum, as revealed by gal4 enhancer trap lines. Front Neural Circuits 3:13.

Scott EK, Mason L, Arrenberg AB, Ziv L, Gosse NJ, Xiao T, Chi NC, Asakawa K, Kawakami K, Baier H (2007) Targeting neural circuitry in zebrafish using GAL4 enhancer trapping. Nat Methods 4:323–326.

Shelly M, Lim BK, Cancedda L, Heilshorn SC, Gao H, Poo MM (2010) Local and long-range reciprocal regulation of cAMP and cGMP in axon/dendrite formation. Science 327:547–552.

Shim S, Zheng JQ, Ming GL (2013) A critical role for STIM1 in filopodial calcium entry and axon guidance. Mol Brain 6:51.

Song HJ, Ming GL, Poo MM (1997) cAMP-induced switching in turning direction of nerve growth cones. Nature 388:275–279.

Song H, Ming G, He Z, Lehmann M, McKerracher L, Tessier-Lavigne M, Poo M (1998) Conversion of neuronal growth cone responses from repulsion to attraction by cyclic nucleotides. Science 281:1515–1518.

Stepanova T, Slemmer J, Hoogenraad CC, Lansbergen G, Dortland B, De Zeeuw CI, Grosveld F, van Cappellen G, Akhmanova A, Galjart N (2003) Visualization of microtubule growth in cultured neurons via the use of EB3-GFP (end-binding protein 3-green fluorescent protein). J Neurosci 23:2655–2664.

Tanaka E, Kirschner MW (1995) The role of microtubules in growth cone turning at substrate boundaries. J Cell Biol 128:127–137.

Terasaki M, Slater NT, Fein A, Schmidek A, Reese TS (1994) Continuous network of endoplasmic reticulum in cerebellar Purkinje neurons. Proc Natl Acad Sci U S A 91:7510–7514.

Thompson AW, Vanwalleghem GC, Heap LA, Scott EK (2016) Functional profiles of visual-, auditory-, and water flow-responsive neurons in the zebrafish tectum. Curr Biol 26:743–754.

Togashi K, von Schimmelmann MJ, Nishiyama M, Lim CS, Yoshida N, Yun B, Molday RS, Goshima Y, Hong K (2008) Cyclic GMP-gated CNG channels function in Sema3A-induced growth cone repulsion. Neuron 58: 694–707.

Tojima T, Akiyama H, Itofusa R, Li Y, Katayama H, Miyawaki A, Kamiguchi H (2007) Attractive axon guidance involves asymmetric membrane transport and exocytosis in the growth cone. Nat Neurosci 10:58–66.

Tojima T, Hines JH, Henley JR, Kamiguchi H (2011) Second messengers and membrane trafficking direct and organize growth cone steering. Nat Rev Neurosci 12:191–203.

Tosney KW, Landmesser LT (1985) Growth cone morphology and trajectory in the lumbosacral region of the chick embryo. J Neurosci 5: 2345–2358.

Tsai FC, Seki A, Yang HW, Hayer A, Carrasco S, Malmersjö S, Meyer T (2014) A polarized $Ca^{2+}$, diacylglycerol and STIM1 signalling system regulates directed cell migration. Nature 16:133–144.

Wang GX, Poo MM (2005) Requirement of TRPC channels in netrin-1-induced chemotropic turning of nerve growth cones. Nature 434:898–904.

Waterman-Storer CM, Salmon ED (1998) Endoplasmic reticulum membrane tubules are distributed by microtubules in living cells using three distinct mechanisms. Curr Biol 8:798–806.

Wen Z, Guirland C, Ming GL, Zheng JQ (2004) A CaMKII/calcineurin

switch controls the direction of Ca(2+)-dependent growth cone guidance. Neuron 43:835–846.

Williamson T, Gordon-Weeks PR, Schachner M, Taylor J (1996) Microtubule reorganization is obligatory for growth cone turning. Proc Natl Acad Sci U S A 93:15221–15226.

Wu Y, Whiteus C, Xu CS, Hayworth KJ, Weinberg RJ, Hess HF, De Camilli P (2017) Contacts between the endoplasmic reticulum and other membranes in neurons. Proc Natl Acad Sci U S A 114:E4859–E4867.

Wyart C, Del Bene F, Warp E, Scott EK, Trauner D, Baier H, Isacoff EY (2009) Optogenetic dissection of a behavioural module in the vertebrate spinal cord. Nature 461:407–410.

Zeller J, Schneider V, Malayaman S, Higashijima S, Okamoto H, Gui J, Lin S, Granato M (2002) Migration of zebrafish spinal motor nerves into the periphery requires multiple myotome-derived cues. Dev Biol 252:241–256.

Zhang H, Hu J (2016) Shaping the endoplasmic reticulum into a social network. Trends Cell Biol 26:934–943.

Zhang XF, Forscher P (2009) Rac1 modulates stimulus-evoked $Ca^{2+}$ release in neuronal growth cones via parallel effects on microtubule/endoplasmic reticulum dynamics and reactive oxygen species production. Mol Biol Cell 20:3700–3712.

Zheng JQ (2000) Turning of nerve growth cones induced by localized increases in intracellular calcium ions. Nature 403:89–93.

Zhou FQ, Zhou J, Dedhar S, Wu YH, Snider WD (2004) NGF-induced axon growth is mediated by localized inactivation of GSK-3beta and functions of the microtubule plus end binding protein APC. Neuron 42:897–912.

Zurek N, Sparks L, Voeltz G (2011) Reticulon short hairpin transmembrane domains are used to shape ER tubules. Traffic 12:28–41.